Chemical Mechanism of a Cysteine Protease, Cathepsin C, As Revealed by Integration of both Steady-State and Pre-Steady-State Solvent Kinetic Isotope Effects

Jessica L. Schneck,[‡] James P. Villa,[‡] Patrick McDevitt,[‡] Michael S. McQueney,[§] Sara H. Thrall,*[,‡] and Thomas D. Meek[‡]

Department of Biological Reagents and Assay Development and Discovery Technology Group, GlaxoSmithKline Pharmaceuticals, 1250 South Collegeville Road, Collegeville, Pennsylvania 19426-0989

Received April 29, 2008; Revised Manuscript Received May 21, 2008

ABSTRACT: Cathepsin C, or dipeptidyl peptidase I, is a lysosomal cysteine protease of the papain family that catalyzes the sequential removal of dipeptides from the free N-termini of proteins and peptides. Using the dipeptide substrate Ser-Tyr-AMC, cathepsin C was characterized in both steady-state and pre-steady-state kinetic modes. The pH(D) rate profiles for both log k_{cat}/K_m and log k_{cat} conformed to bell-shaped curves for which an inverse solvent kinetic isotope effect (sKIE) of 0.71 ± 0.14 for $^{D}(k_{cat}/K_a)$ and a normal sKIE of 2.76 ± 0.03 for $^{D}k_{cat}$ were obtained. Pre-steady-state kinetics exhibited a single-exponential burst of AMC formation in which the maximal acylation rate (k_{ac} = 397 ± 5 s^{-1}) was found to be nearly 30-fold greater than the rate-limiting deacylation rate (k_{dac} = 13.95 ± 0.013 s^{-1}) and turnover number (k_{cat} = 13.92 ± 0.001 s^{-1}). Analysis of pre-steady-state burst kinetics in D_2O allowed abstraction of a normal sKIE for the acylation half-reaction that was not observed in steady-state kinetics. Since normal sKIEs were obtained for all measurable acylation steps in the presteady state [$^{D}k_{ac}$ = 1.31 ± 0.04, and the transient kinetic isotope effect at time zero ($tKIE^0$) = 2.3 ± 0.2], the kinetic step(s) contributing to the inverse sKIE of $^{D}(k_{cat}/K_a)$ must occur more rapidly than the experimental time frame of the transient kinetics. Results are consistent with a chemical mechanism in which acylation occurs via a two-step process: the thiolate form of Cys-234, which is enriched in D_2O and gives rise to the inverse value of $^{D}(k_{cat}/K_a)$, attacks the substrate to form a tetrahedral intermediate that proceeds to form an acyl−enzyme intermediate during a proton transfer step expressing a normal sKIE. The subsequent deacylation half-reaction is rate-limiting, with proton transfers exhibiting normal sKIEs. Through derivation of 12 equations describing all kinetic parameters and sKIEs for the proposed cathepsin C mechanism, integration of both steady-state and pre-steady-state kinetics with sKIEs allowed the provision of at least one self-consistent set of values for all 13 rate constants in this cysteine protease's chemical mechanism. Simulation of the resulting kinetic profile showed that at steady state ~80% of the enzyme exists in an active-site cysteine-acylated form in the mechanistic pathway. The chemical and kinetic details deduced from this work provide a potential roadmap to help steer drug discovery efforts for this and other disease-relevant cysteine proteases.

Over the past 14 years, members of the cathepsin family have been heavily explored as drug targets due to their implication in a variety of disease states, including osteoporosis and osteoarthritis (cathepsin K, B, and L), Alzheimer's disease (cathepsin L, B, and S), tumor invasion and metastasis (cathepsin B, L, H, and K), muscular dystrophy (cathepsin L and B), and emphysema (cathepsin S and K) (*1*). Of these, cathepsin K has been the most actively pursued, on the basis, in part, of human target validation derived from studies of patients with pycnodysostosis, a rare genetic disease characterized by a reduction in bone resorption and caused by loss of function mutations in the cathepsin K gene (*2*). Intensive medicinal chemistry efforts directed at cathepsin K have produced only two drug candidates that have reached phase II clinical studies (*3, 4*).

Cathepsin C is another member of this papain-like cysteine protease family that only recently has been drawing an increasing amount of interest as a therapeutic target. Mice containing cathepsin C gene deletions show protection in models of inflammatory diseases such as acute inflammatory arthritis, sepsis, and abdominal aortic aneurysm (*5–7*). The protection imparted on cathepsin C knockout mice in these disease models is thought to derive from its role in activating leukocyte and mast cell granule serine proteases (*5, 8*). Similar to cathepsin K, genetic mutations resulting in deficiencies in cathepsin C activity have been identified in humans. Loss of function mutations in cathepsin C result in Papillon-Lefevre or Haim-Munk syndrome, each of which is characterized by palmoplantar keratoderma and early onset periodontitis (*9, 10*).

The main challenge for cathepsin-directed medicinal chemistry efforts derives from the fact that the majority of inhibitors that have been identified contain an electrophilic "warhead", such as a nitrile or ketone group, which reacts with the active-site cysteine nucleophile. Compounds con-

* To whom correspondence should be addressed. Phone: (610) 917-6773. Fax: (610) 917-7385. E-mail: Sara.H.Thrall@gsk.com.
[‡] Department of Biological Reagents and Assay Development.
[§] Discovery Technology Group.

10.1021/bi8007627 CCC: $40.75
Published on Web 07/26/2008

taining nitriles may also react irreversibly with other cysteines depending on the degree of their electrophilicity (*11*). Electrophilic compounds or metabolites are believed to mediate drug-related adverse events, and therefore, such groups are generally undesirable in drug candidates (*12*).

The chemical mechanism of cysteine proteases has been extensively characterized by means of kinetic and structural studies (*13–27*). A double-displacement mechanism involving the formation of an acyl−enzyme intermediate has been conclusively demonstrated for papain-like cysteine proteases. The majority of these mechanistic studies have comprised pH−rate profiles (*14–20*), covalent inactivation studies (*15, 16, 19, 20*), sensitivity to inhibitors (*24*), and identification of catalytic groups by mutational analysis (*23*). Pre-steady-state kinetic evaluations of papain-like cysteine proteases have been infrequently reported, but a few reports suggest that deacylation is the rate-limiting step for some substrates in catalysis (*25, 26*). In addition, inverse sKIEs[1] were demonstrated for the acylation half-reaction for papain for selected substrates (*14, 19*), aldehyde inactivators (*24*), and covalent modifying agents (*15, 20*). The current view from all of these studies is that cysteine proteases employ a catalytic dyad composed of the thiolate−imidazolium species of the conserved Cys and His residues found in their active sites, although the protonation states of these catalytic groups have been the subject of considerable debate (*15, 24, 27*).

In this study, we embarked on combining transient and steady-state kinetics with deuterium solvent kinetic isotope effects to develop a comprehensive chemical mechanism for cathepsin C. We were able to provide values for the collections of individual rate constants in the mechanistic pathway by the simultaneous solution of the mathematical expressions for the experimental kinetic parameters obtained under transient and steady-state conditions. With the improved understanding of the kinetic and chemical mechanism in this study, new approaches to the screening for, or rational design of, potent and specific cathepsin inhibitors that are less reactive and perhaps devoid of an electrophilic center may be explored.

EXPERIMENTAL PROCEDURES

Materials. Deuterated water (D_2O), deuterium chloride (DCl), and sodium deutroxide (NaOD) were purchased from Sigma-Aldrich (≥99 at. % ^2H). SY-AMC was purchased from MP Biomedicals. Sodium hydroxide, hydrochloric acid, CHAPS, DTT, and EDTA were purchased from Sigma-Aldrich. Sodium chloride and anhydrous sodium acetate were purchased from Mallinckrodt. MES was purchased from J. T. Baker. Triethanolamine was purchased from Fluka Biochemika. DMSO (99.97% pure, chromatography grade) was purchased from EMD Biosciences. The mechanism-based inactivator of cathepsin C, Ala-Hph-VS-Ph, was prepared as described previously (*28*).

Cloning, Expression, and Purification of Cathepsin C. A construct within a pCDN vector comprising human pre-pro-cathepsin C, a TEV processing sequence, and an IgG-Fc domain at the C-terminus was cloned and expressed in a CHO cell line with a glycosylation-deficient phenotype (*29*). Pre-pro-cathepsin C was captured by affinity chromatography on immobilized Protein A (*30*), and the acid eluate was dialyzed against sodium citrate buffer (pH 4.5). Concerted activation of cathepsin C and removal of the Fc fusion partner were carried out by proteolysis with recombinant cathepsin L. Mature active cathepsin C was purified from the byproducts of cathepsin L processing, by size exclusion chromatography on Superdex 200 into sodium phosphate, EDTA buffer (pH 6−7). Purity was determined to be ~95% by SDS−PAGE, which under reducing conditions separated the protein into three constituents. Three N-termini were found by Edman N-terminal sequence analysis, DTPANXTYLD, ILHLPTSWDWR, and DPFNPFELTN, which correspond to the exclusion domain, heavy chain, and light chain, respectively (*47*).

Steady-State Kinetics. Initial rates of the peptidolytic reaction catalyzed by cathepsin C were typically measured in 10.5 μL reaction mixtures in 384-well Greiner polypropylene low-volume plates, containing 50 mM sodium acetate (pH 5.6; 21 ± 1 °C), 30 mM NaCl, 1 mM EDTA, 1 mM CHAPS, 1 mM DTT (buffer A), and 0.5 μL of 0.005−1.05 mM SY-AMC, delivered by 2-fold dilutions of solutions of 100% (v/v) DMSO. Reactions were initiated by addition of 0.5 μL of SY-AMC to a 10 μL solution containing 20 pM cathepsin C in buffer A, followed by fluorescence measurement of free AMC production using an Acquest fluorimeter (Molecular Devices), with sampling every 60 s for up to 3600 s with 360 nm excitation, 460 nm emission, and 400 nm cutoff filters.

Active-Site Titration. Concentrations of active sites in preparations of cathepsin C were determined by measurement of residual enzyme activity following preincubation of the enzyme with a potent, irreversible inactivator Ala-Hph-VS-Ph (*28*), by the method of Grant et al. (*31*). Results indicated preparations of cathepsin C contained 0.92 active site per monomer (data not shown).

pH−Rate Profiles and Solvent Kinetic Isotope Effects. The pH dependence of k_{cat}/K_m (V/K) and k_{cat} (V/E_t) for SY-AMC was investigated by measurement of initial rates over the pH range of 3.5−8, in increments of 0.3 pH unit, in a mixed buffer consisting of 100 mM sodium acetate, 100 mM MES, 50 mM triethanolamine, 1 mM DTT, and 1 mM CHAPS [buffer B, constant ionic strength $I = 0.10$ (*32*)]. pH values were adjusted with small aliquots of concentrated HCl or NaOH. To measure the sKIE over an identical range of pD values, k_{cat}/K_m and k_{cat} for SY-AMC were determined as described above over the pD range of 3.5−8 in buffer B prepared in deuterium oxide, with pD values in increments of 0.3 pD unit adjusted via addition of minimal volumes of DCl or NaOD, yielding final reaction mixtures containing 93.54 ± 0.05% (v/v) deuterium oxide. The content of deuterium in these buffers was quantified by proton NMR analysis of the water and DMSO peaks in five buffer samples. Values of pD were determined as $pD = pH_{measured} + 0.35$, according to the method of Schowen and Schowen (*33*).

Pre-Steady-State Burst Kinetics. Evaluation of pre-steady-state kinetics of cathepsin C was conducted in buffer A [pH(D) 5.6], at 21 ± 1 °C in H_2O or D_2O, and at 40−51 nM cathepsin C with 1−30 μM SY-AMC. Time courses (0.002−0.2 s) of AMC production were determined using

[1] Abbreviations: AMC, 7-amino-4-methylcoumarin; CHO, Chinese hamster ovary; SY-AMC, serine-tyrosine-4-amino-7-methylcoumarin; MES, 2-(*N*-morpholino)ethanesulfonic acid; DTT, dithiothreitol; CHAPS, 3-[3-(cholamidopropyl)dimethylammonio]-1-propanesulfonate; DMSO, dimethyl sulfoxide; EDTA, ethylenediaminetetraacetic acid; sKIE, solvent kinetic isotope effect(s); Ala-Hph-VS-Ph, 3-(*N*-alanyl)amino-5-phenyl-1-(phenylsulfonyl)-1-pentene (hydrochloride); TEV, tobacco etch virus; tKIE, transient kinetic isotope effect.

Scheme 1: Proposed Mechanism of Cathepsin C[a]

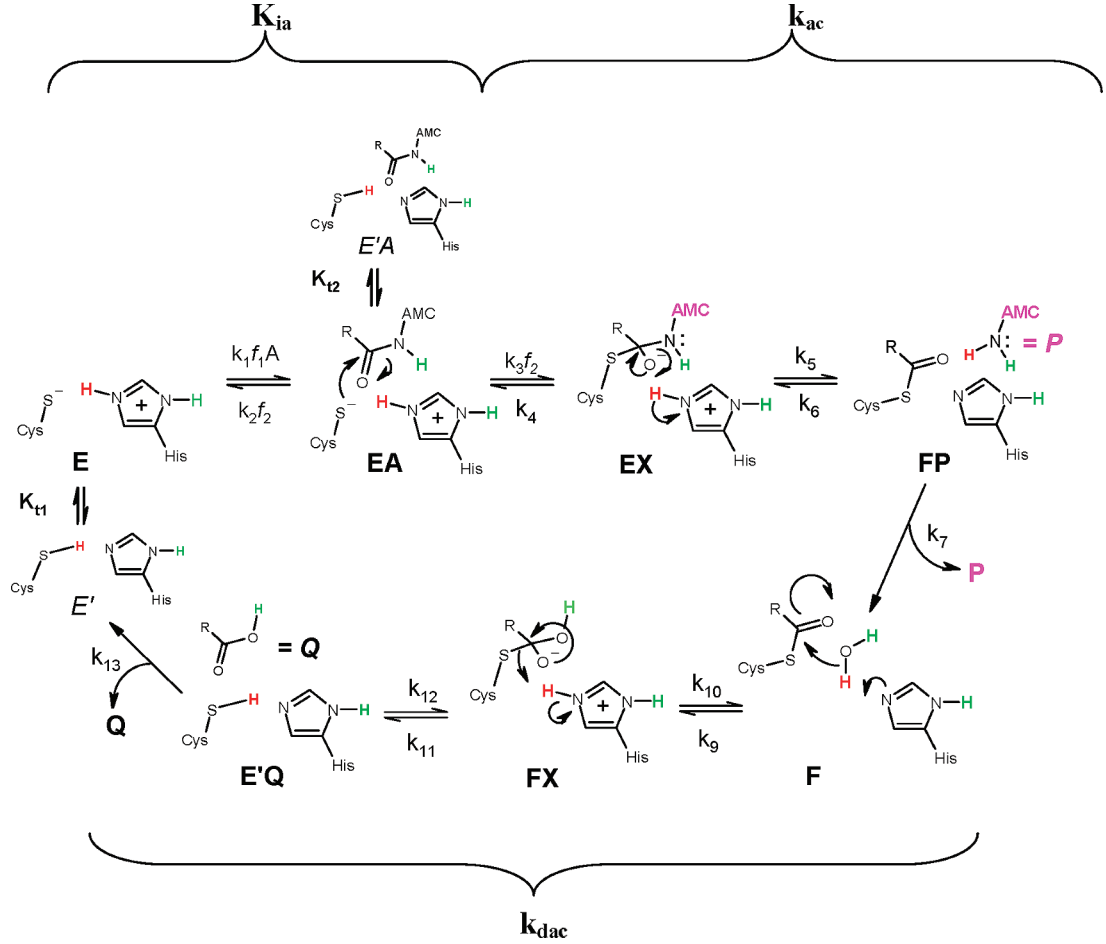

[a] K_{ia} is the dissociation constant for the substrate Ser-Tyr-AMC (A) binding to free enzyme, and k_{ac} and k_{dac} are the rates of acylation and deacylation, respectively, with saturating substrate. K_{t1}, K_{t2}, f_1, and f_2 are explained in the theory section. Protons expected to contribute to primary (red) and secondary (green) sKIEs are indicated for the germane reaction steps. AMC is colored pink to denote the generation of the fluorescence signal measured in this work.[2]

an Applied Photophysics SX20 stopped-flow spectrophotometer, where fluorescence readings (excitation at 348 nm, emission at 438 nm, and 400 nm cutoff filter) were collected by computer and analyzed with Pro Data SX. For calibration of the stopped-flow spectrophotometer, two sample syringes, containing buffer A (syringe A) and a single concentration of SY-AMC (syringe B), were maintained at room temperature prior to being mounted on the stopped-flow apparatus. For each concentration of SY-AMC, the concentration of any contaminating free AMC was determined by rapid mixing of the contents of two syringes and subsequent measurement of the fluorescence time course. A calibration curve was generated, from which contaminating quantities of AMC were determined and used to correct the signal for the enzyme time courses. For experimental samples, syringe A contained cathepsin C (92−102 nM in buffer A in H_2O or D_2O), and time courses were obtained at 1−30 μM SY-AMC. Fluorescence time courses were comprised of 10000 time points for each fixed concentration of SY-AMC, and time courses of AMC formation in millivolts of fluorescence were converted to nanomolar concentrations of product formed following calibration of the system with known levels of AMC. All time courses were analyzed as either single- or double-exponential functions and were determined in triplicate for each fixed concentration of SY-AMC.

Data Analysis. Kinetic data were fitted to appropriate rate equations using the nonlinear regression function of SigmaPlot 2000 version 9.1 (SPSS, Inc.).

Initial rate data were fitted to eq 1 to determine the kinetic parameters k_{cat} and k_{cat}/K_a.

$$v = k_{cat}E_tA/(K_a + A) \quad (1)$$

For eq 1, v is the initial rate, k_{cat} is the turnover number, E_t is the concentration of active sites of cathepsin C, and K_a is the Michaelis constant for substrate A.

Data for all pH profiles were fitted to eqs 2 and 3, in which y is the observed kinetic parameter k_{cat}/K_a or k_{cat}, c is the pH-independent value of y, H is the hydrogen ion concentration, and K_1-K_3 are apparent acid or base dissociation constants. The sKIEs were calculated from the pH(D)-independent values, c_H or c_D of k_{cat}/K_a and k_{cat}, as obtained from eq 2 or 3, by use of eq 4 to solve for E_c (the isotope effect minus 1), and via correction for the fraction of D_2O (F_i) used in the studies. Error propagation on calculated values of the sKIE was determined from the ratios of the experimental values in H_2O and D_2O, by the use of eq 5, where δc_H, δc_D, and δc_{F_i} are experimental standard deviations of c_H, c_D, and F_i, respectively, and $\partial f/\partial c_H$, $\partial f/\partial c_D$, and $\partial f/\partial c_{F_i}$ are the partial derivatives of the left-hand side of eq 4.

$$\log y = \log[c/(1 + H/K_1 + K_2/H)] \quad (2)$$

$$\log y = \log\{c/[1 + H/K_1 + (K_2/H)(1 + K_3/H)]\} \quad (3)$$

$$(c_H/c_D - 1)/F_i = E_c \quad (4)$$

$$\text{Errorprop} = \delta c_H(\partial f/\partial c_H) + c_D(\partial f/\partial c_D) + c_{F_i}(\partial f/\partial c_{F_i}) \quad (5)$$

Pre-steady-state data were fitted to eqs 6 and 7 for each fixed concentration of SY-AMC, which describe time courses conforming to single- and double-exponential functions (*34*), respectively, for which [P] is AMC formed (bound or free, nanomolar), k_{ss} is the apparent steady-state rate, t is time (seconds), β is the apparent burst amplitude, λ is the apparent rate of the exponential phase, and C is a constant of calibration (*34*).

$$[P] = k_{ss}E_t(t) + \beta E_t[1 - \exp(-\lambda t)] + C \quad (6)$$

$$[P] = k_{ss}E_t(t) + \beta_1 E_t[1 - \exp(-\lambda_1 t)] + \beta_2 E_t[1 - \exp(-\lambda_2 t)] + C \quad (7)$$

Additionally, pre-steady-state data conforming to a single-exponential function were fitted globally to eq 8, in which more than 200000 data points representing pre-steady-state time courses for all fixed concentrations of SY-AMC were simultaneously fitted, where [P] is the concentration of AMC formed (micromolar), A is the fixed concentration of SY-AMC (5−30 μM), E_t is the enzyme concentration (0.046−0.051 μM), t is time (seconds), k_{cat}, k_{ac}, and k_{dac} are turnover numbers for the full reaction and the acylation and deacylation half-reactions, respectively, in units of inverse seconds, and $K_{a'}$ and K_{ia1} are a pseudo-Michaelis constant and an apparent dissociation constant for SY-AMC, respectively (micromolar) (see the next section).

$$[P] = k_{cat}AE_t(t)/(K_{a'} + A) + [k_{cat}A/k_{dac}(K_{a'} + A)]^2E_t \times (1 - \exp(-(t)\{[(k_{ac} + k_{dac})A + k_{dac}K_{ia1}]/(A + K_{ia1})\}) \quad (8)$$

In all cases, the most appropriate fit for each equation was determined by an *F*-test analysis of the results of nonlinear regression.

Nomenclature. Isotope effects are expressed using the notation of Cook, Cleland, and Northrop (*41, 42*). Solvent kinetic and equilibrium isotope effects measured on the kinetic parameters k_{cat} and k_{cat}/K_a are notated as leading superscripts, defined as D for simplicity, with the variable substrate as the right subscript.

Theory Underlying the Derivation of the Steady-State and Pre-Steady-State Kinetic and sKIE Expressions. To analyze solvent kinetic isotope effects for cathepsin C in both steady-state and pre-steady-state modes, we first considered the generally accepted, double-displacement mechanism employed by cysteine proteases shown in Scheme 1, for which K_{ia} is the dissociation constant for the substrate (A) binding to free enzyme and k_{ac} and k_{dac} are the rates of acylation and deacylation, respectively, with saturating substrate. Protons expected to contribute to primary (red) and secondary (green) sKIEs are indicated for the germane reaction steps.

As shown in Scheme 1, when substrate binds, attack of the thiolate in EA on the scissile carbonyl group of Ser-Tyr-AMC (A) leads to covalent tetrahedral intermediate EX, which collapses to the acylated enzyme form F following proton transfer from the imidazolium group to the departing amine, AMC (P). In the second half-reaction, the active-site imidazole group deprotonates the lytic H_2O, which concomitantly attacks the carbonyl of the acyl group in F to form the second tetrahedral intermediate in FX. Collapse of this intermediate with attending proton transfer from the imidazolium group to the sulfur leads to the formation of the Ser-Tyr-COOH product (Q) and free enzyme form E′. When hydrolysis of acyl−enzyme F is significantly slower than its formation, under pre-steady-state conditions the time course of production of product P will constitute a burst, which can be observed when P is a fluorescent or chromophoric species in the EX and FP complexes, or as free P.[2]

To derive the steady-state and pre-steady-state equations describing the mechanism in Scheme 1, the protonation states of the active-site Cys and His of cathepsin C needed to be considered. The protonation states are depicted in Scheme 1 as tautomeric forms in the E, EA, E′, and E′A species for which the catalytically viable species E and EA contain thiolate and imidazolium ions in the active site, and from which $K_{t1} = [E']/[E]$ and $K_{t2} = [E'A]/[EA]$. The fractional component of each of the enzyme tautomers that proceed through an individual kinetic step is given by the equation $f_1 = [E]/([E'] + [E]) = 1/(K_{t1} + 1)$ or $f_2 = [EA]/([E'A] + [EA]) = 1/(K_{t2} + 1)$ such that, for example, the overall rate of substrate binding to the competent enzyme form E is given by $k_1(E)(A)/(1 + K_{t1})$. The value of K_{t1} has been shown to be equal to ≤0.5 for unsubstituted papain (*15, 18*) but may be highly dependent on the cysteine protease and experimental conditions in question.

Steady-State Expressions. The concentrations of reactive species E and EA equal $E_t/(1 + K_{t1})$ and $E_t/(1 + K_{t2})$ at low and high levels of A, respectively. The steady-state equations may then be written using the method of net rate constants (*35*) in eqs 9–12, for which the rate constants k_1f_1, k_2f_2, and k_3f_2 are written as $k_1/(1 + K_{t1})$, $k_2/(1 + K_{t2})$, and $k_3/(1 + K_{t2})$, respectively.

$$v = E_t/(\{k_2[k_4(k_6 + k_7) + k_5k_7] + k_3k_5k_7\}(1 + K_{t1})/k_1k_3k_5k_7A + [k_4(k_6 + k_7) + k_5k_7](1 + K_{t2})/k_3k_5k_7 + (k_6 + k_7)/k_5k_7 + 1/k_7 + [k_{10}(k_{12} + k_{13}) + k_{11}k_{13}]/k_9k_{11}k_{13} + (k_{12} + k_{13})/k_{11}k_{13} + 1/k_{13}) \quad (9)$$

$$k_{cat} = k_5K_{eq3}E_t/\{(1 + K_{t2})(1 + b + c) + K_{eq3}(1 + c + e) + (k_5K_{eq3}/k_9)[1 + z(1 + y + w) + x(1 + y)]\} \quad (10)$$

$$k_{cat}/K_a = k_5K_{eq3}E_t/\{(1 + K_{t1})K_{ia}[1 + b(1 + a) + c]\} \quad (11)$$

where

$$K_{ia1} = k_2f_2/k_1f_1 \quad K_{ia} = k_2/k_1 \quad K_{eq3} = k_3/k_4$$
$$a = k_3/k_2 \quad b = k_5/k_4 \quad c = k_6/k_7 \quad d = k_3/k_5$$
$$e = k_5/k_7 \quad x = k_{10}/k_{11} \quad y = k_{12}/k_{13} \quad z = k_9/k_{11}$$
$$w = k_{11}/k_{13} \quad (12)$$

[2] Although unproven here, the formation of the tetrahedral intermediate in the EX complex could produce a fluorescent signal as the lone pair of electrons on the scissile nitrogen atom of AMC in this complex is now available for establishing resonance with the methylcoumarin moiety. From this, it is possible that both the EX and FP complexes contribute to the total fluorescent signal in the transient kinetics, as both would have bound fluorescent species. Accordingly, it was found that the time course simulations shown in Figures 5 and 6 overlap more closely with the data in the first 20 ms when the fluorescence signal is comprised of EX in addition to FP and P.

Table 1: Initial Rate Data, pK Values, and Steady-State Solvent Kinetic Isotope Effects for Cathepsin C[a]

solvent	k_{cat}/K_a (μM^{-1} s^{-1})	pK value (k_{cat}/K_a)	k_{cat} (s^{-1})	pK value (k_{cat})	K_a (μM)	solvent kinetic isotope effect[b]
H_2O[c]	0.35 ± 0.03	N/A	2.4 ± 0.03	N/A	6.9 ± 0.2	N/A
H_2O	0.40 ± 0.035	$pK_1 = 4.3 \pm 0.1$ $pK_2 = 6.5 \pm 0.1$ $pK_3 = 7.7 \pm 0.7$	2.38 ± 0.05	$pK_4 = 3.52 \pm 0.02$ $pK_5 = 7.7 \pm 0.1$	6.0 ± 0.2	$^D(k_{cat}/K_a) = 0.71 \pm 0.14$
D_2O	0.54 ± 0.05	$pK_1 = 4.85 \pm 0.07$ $pK_2 = 6.9 \pm 0.11$	0.88 ± 0.02	$pK_4 = 3.43 \pm 0.06$ $pK_5 = 7.9 \pm 0.2$	1.7 ± 0.3	$^Dk_{cat} = 2.76 \pm 0.03$

[a] N/A, not applicable. Data obtained from fits of initial rate data to eq 1 and pH(D)−rate profile data to eqs 2 and 3. [b] sKIEs were calculated from the pH(D)-independent values of k_{cat}/K_a and k_{cat} obtained from c values in eqs 2 and 3, which were then fitted to eqs 4 and 5. [c] Data from pH 5.6.

At saturating concentrations of substrate A, the steady-state rates for the acylation and deacylation half-reactions are described by eqs 13a and 13b, respectively.

$$k_{ac-ss} = k_5K_{eq3}E_t/[(1 + K_{t2})(1 + b + c) + K_{eq3}(1 + c + e)] \quad (13a)$$

$$k_{dac} = k_9E_t/[1 + z(1 + y + w) + x(1 + y)] \quad (13b)$$

We next considered the effect of deuterium oxide on the concentrations of enzyme species E, E′, EA, and E′A in Scheme 1. As the fractionation factor for sulfhydryl groups is less than 1 [$\phi_{SL} = 0.4-0.5$ (*33, 36*)] and since the solvent equilibrium isotope effect on the values of K_{t1} and K_{t2} will be a ratio of the fractionation factors for sulfhydryl and imidazole/imidazolium species, or $^DK_t = [\text{R-SD}][\text{R-ND}_2^+][\text{RNH}]/([\text{R-SH}][\text{R-NH}_2^+][\text{RND}]) = (\phi_{NL}^+)^2/[(\phi_{SL})(\phi_{NL})] = (1.08)^2/[(0.4)(1.12)] = 2.56$ (*33, 36*), it follows that the E and EA species will be enriched in D_2O (*15–18, 36, 37*), and this could result in an inverse isotope effect on k_{cat}/K_a. Accordingly, the ratio of active enzyme species E in D_2O compared to H_2O, $[E]_{H_2O}/[E]_{D_2O}$, is given by $(1 + K_{t1}/^DK_t)/(1 + K_{t1})$. It is clear from this expression that the ratio $[E]_{H_2O}/[E]_{D_2O}$ will vary from 1 to 0.7 as the value of K_{t1} varies from 0 to 1, indicating that the magnitude of any inverse solvent isotope effect on k_{cat}/K_a will depend on the value of K_{t1}.

Considering from Scheme 1 that primary sKIEs are likely present on the k_5, k_9, and k_{11} steps, the steady-state expressions for solvent isotope effects for k_{cat}/K_a, k_{cat}, and k_{dac} may be found with eqs 14–16:

$$^D(k_{cat}/K_a) = [(1 + K_{t1}/^DK_t)/(1 + K_{t1})][^Dk_5 + b(1 + a) + c^DK_{eq5}]/[1 + b(1 + a) + c] \quad (14)$$

$$^Dk_{cat} = \{[(1 + K_{t2}/^DK_t)(^Dk_5 + b + c^DK_{eq5}) + K_{eq3}(^Dk_5 + c^DK_{eq5} + e)] + (k_5K_{eq3}/k_9)[^Dk_9 + z(^Dk_{11} + y^DK_{eq11} + w) + x(^Dk_{11}{}^DK_{eq9} + y^DK_{eq9}{}^DK_{eq11})]\}/\{(1 + c + b)(1 + K_{t2}) + K_{eq3}(1 + c + e) + (k_5K_{eq3}/k_9)[1 + z(1 + y + w) + x(1 + y)]\} \quad (15)$$

$$^Dk_{dac} = [^Dk_9 + z(^Dk_{11} + y^DK_{eq11} + w) + x(^Dk_{11}{}^DK_{eq9} + y^DK_{eq9}{}^DK_{eq11})]/[1 + z(1 + y + w) + x(1 + y)] \quad (16)$$

Pre-Steady-State Kinetic Expressions. To derive expressions for the pre-steady-state kinetics of the cathepsin C reaction, we simplified the mechanism in Scheme 1 by assuming that the conversion of the EA complex to EX, which is attack of the active-site cysteine on the bound substrate, is very rapid. This means that at high values of substrate A, the enzyme complexes E′A, EA, and EX may be represented as a single species in equilibrium for which $f_5 = [EX]/([EA] + [E'A] + [EX]) = K_{eq3}/(1 + K_{t2} + K_{eq3})$ and $K_{eq3} = k_3/k_4$. The transient rate of acylation, k_{ac}, for which $E_t = [EA:F] = [EA] + [E'A] + [EX] + [FP] + [F]$ and which involves the k_3, k_5, and k_7 steps, is described by eq 17.

$$k_{ac} = E_t/(1/k_5f_5 + 1/k_{7'}) = [k_5k_7f_5E_t/(k_5f_5 + k_6 + k_7)] = k_5K_{eq3}E_t/[(1 + K_{t2} + K_{eq3})(1 + k_6/k_7) + k_5K_{eq3}/k_7] \quad (17)$$

Assuming that any contributions from secondary sKIEs to the k_3 step are negligible, the sKIE on the transient rate of acylation is given by eq 18.

$$^Dk_{ac} = \{[^Dk_5 + (k_6/k_7)^DK_{eq5}](1 + K_{t2}/^DK_t + K_{eq3}) + k_5K_{eq3}/k_7\}/[(1 + K_{t2} + K_{eq3})(1 + k_6/k_7) + k_5K_{eq3}/k_7] \quad (18)$$

Accordingly, the following expressions (eqs 19a–19e) describe the formation of species E, EA:F, and F in the presteady state, for the mechanism of Scheme 1.

$$d(E)/dt = -k_1f_1A(E) + k_2f_2(EA:F) + k_{dac}(F) \quad (19a)$$

$$d(EA:F)/dt = k_1f_1A(E) - (k_2f_2 + k_{ac})(EA:F) \quad (19b)$$

$$d(F)/dt = k_{ac}(EA:F) - k_{dac}(F) \quad (19c)$$

$$dQ/dt = k_{dac}(F) \quad (19d)$$

$$E_t = [E] + [EA:F] + [F] \quad (19e)$$

Solutions for $(F)_t$ from eqs 19a–19e are found in eqs 20–24 and were obtained using the conventions of Moore and Pearson (*38*) and Johnson (*34*).

$$(F)_t = A_0\{1 + [\lambda_2/(\lambda_1 - \lambda_2)]e^{-\lambda_1t} - [\lambda_1/(\lambda_1 - \lambda_2)]e^{-\lambda_2t}\} \quad (20)$$

where

$$A_0 = k_1f_1k_{ac}AE_t/[k_1f_1A(k_{ac} + k_{dac}) + k_{dac}(k_2f_2 + k_{ac})] \quad (21)$$

$$\lambda_{1,2} = (k_1f_1A + k_2f_2 + k_{ac} + k_{dac})/2 \pm [(k_1f_1A + k_2f_2 + k_{ac} + k_{dac})^2 - 4(k_1f_1k_{ac}A + k_{dac}(k_1f_1A + k_2f_2 + k_{ac}))]^{1/2}/2 \quad (22)$$

$$\lambda_1 \cong [k_1f_1k_{ac}A + k_{dac}(k_1f_1A + k_2f_2 + k_{ac})]/(k_1f_1A + k_2f_2 + k_{ac} + k_{dac}) \quad (23)$$

$$\lambda_2 \cong k_1f_1A + k_2f_2 + k_{ac} + k_{dac} \quad (24)$$

The equation for the observed pre-steady-state burst is ascertained by substitution of eqs 20–24 into eq 19d, and integration, to yield eq 25.

$$Q_t = k_{dac}A_0(t) + k_{dac}A_0\{\lambda_2/[\lambda_1(\lambda_1 - \lambda_2)]\}(1 - e^{-\lambda_1t})\} - k_{dac}A_0\{[\lambda_1/[\lambda_2(\lambda_1 - \lambda_2)]\}(1 - e^{-\lambda_2t})\}$$
$$= k_1f_1k_{ac}k_{dac}A(t)E_t/[k_1f_1A(k_{ac} + k_{dac}) + k_{dac}(k_2f_2 + k_{ac})] + \beta_1(1 - e^{-\lambda_1t}) - \beta_2(1 - e^{-\lambda_2t}) \quad (25)$$

Equation 25 describes a pre-steady-state burst with two exponential components and is the same in form as eq 7, where

$$\beta_1 = k_1 f_1 k_{ac} k_{dac} A E_t (k_1 f_1 A + k_2 f_2 + k_{ac} + k_{dac}) / [k_1 f_1 A (k_{ac} + k_{dac}) + k_{dac}(k_2 f_2 + k_{ac})]^2 \quad (26)$$

$$\beta_2 = k_1 f_1 k_{ac} k_{dac} A E_t / (k_1 f_1 A + k_2 f_2 + k_{ac} + k_{dac})^3 \quad (27)$$

Note that under conditions where $k_1 f_1 A$ and $k_2 f_2 > k_{ac}$, eq 25 may be written as eq 28, which has the same form as eq 8 and contains the parameters given in eqs 29–33.

$$Q_t = k_{ss} E_t(t) + (\beta_1 - \beta_2)(1 - e^{-\lambda_1 t}) \quad (28)$$

$$k_{ss} = k_{cat} A / (K_{a'} + A) = k_{ac} k_{dac} A / [(k_{ac} + k_{dac})(K_{a'} + A)] \quad (29)$$

$$K_{a'} = k_{dac}(K_{ia1} + k_{ac}/k_1 f_1) / (k_{ac} + k_{dac}) \quad (30)$$

$$\lambda_1 = [A(k_{ac} + k_{dac}) + k_{dac} K_{ia1}] / (A + K_{ia1}) \quad (31)$$

$$\beta_1 - \beta_2 \cong (k_{ac} k_{dac} A)^2 E_t / [k_{dac}(k_{ac} + k_{dac})(A + K_{a'})]^2 \quad (32)$$

$$K_{ia1} = K_{ia}(1 + K_{t1}) / (1 + K_{t2}) \quad (33)$$

Expressions for Transient Kinetic Isotope Effects. We employed the conventions of Palfey and Fagan (*39*) and Maniscalco et al. (*40*) to generate expressions for the transient kinetic isotope effect, tKIE, which may be determined at the limit of time zero, or tKIE°. For the mechanism in Scheme 1, we expect to observe a tKIE on the k_5 step and an equilibrium isotope effect on the tautomeric equilibrium for the E and E′ species, K_{t1}.

We evaluated the tKIE as $t \rightarrow 0$ ($tKIE°_{FP}$) on the kinetic steps in which the formation of FP is described by eq 34 according to the method of Palfey and Fagan (*39*), for which only the concentrations of E and E′ are non-zero as $t \rightarrow 0$.

$$tKIE°_{FP} = \lim_{t \rightarrow 0} [d(FP)_{H_2O}/dt] / [d(FP)_{D_2O}/dt] = k_5 (E)_{H_2O} / [(k_5/{}^D k_5)(E)_{D_2O}] \quad (34)$$

which may be expressed as eq 35.

$$tKIE°_{FP} = \lim_{t \rightarrow 0} [d(FP)_{H_2O}/dt] / [d(FP)_{D_2O}/dt] = {}^D k_5 (1 + K_{t1}/{}^D K_t) / (1 + K_{t1}) \quad (35)$$

Data Fitting and Simulations. Simultaneous solution of the 12 equations describing all values of the kinetic parameters, the intrinsic kinetic and equilibrium isotope effects, the ratios of the individual rate constants, and the ratios of the tautomeric forms of the enzyme (K_{t1} and K_{t2}) was done by using the Levenberg−Marquardt algorithm as implemented by the NLIN procedure in SAS (version 9.1.3 on a Service Pack 2 on a XP Pro Platform; Cary, NC). The NLIN procedure produces least-squares or weighted least-squares estimates of parameters for a nonlinear model from estimation of the variables. Values for all 13 rate constants (k_1−k_{13}) in Scheme 1 and Table 3 determined by the simultaneous fitting were entered into the program Scientist (MicroMath Scientist for Windows, version 2.01), using the model described in Scheme 1. Simulations of the time courses for the formation and disintegration of all enzyme species shown in Scheme 1 during catalysis were then derived using substrate and enzyme concentrations described in this work.

RESULTS AND DISCUSSION

Steady-State Kinetics of Cathepsin C: Initial Rate Data and pH−Rate Profiles. Initial rate data of cathepsin C-catalyzed hydrolysis of SY-AMC (0.024−50.0 μM) at pH 5.6 exhibited classical Michaelis−Menten behavior (data not shown) and were fitted to eq 1, yielding the values of k_{cat}/K_a, k_{cat}, and K_a summarized in Table 1. The pH−rate profiles over a pH 3.5−8.0 range are shown in Figure 1 with results also summarized in Table 1. The plot of log k_{cat}/K_a versus pH comprised a bell-shaped curve in which the value of k_{cat}/K_a decreased at both acidic and basic pH values with asymptotic slopes of 1 and −2, respectively. Accordingly, these data fit better to eq 3 than eq 2 (according to *F*-test results, $p < 0.05$). The data for log k_{cat}/K_a conformed to a model in which a single residue on the enzyme must remain unprotonated for substrate binding and catalysis, and two other residues must be protonated, where it is assumed that these p*K* values represent enzymatic groups on the free form of the enzyme as p*K* values for groups on the dipeptide substrate would be outside the experimental pH range of these studies. The pH−rate profile for k_{cat}/K_a and the corresponding p*K* values are highly similar to those observed for human kidney cathepsin C using the substrate Gly-Phe-4-methoxy-β-naphthylamide [p*K* values of 4.2 ± 0.05, 6.8 ± 0.1, and 7.7 ± 0.1 (*43*)] and somewhat similar to those observed for papain using *N*-carbobenzoxyglycine *p*-nitrophenyl ester as a substrate [p*K* values of 4.5 ± 0.1 and 8.8 ± 0.1 (*19*)]. The similar p*K* values from the plot of log k_{cat}/K_a versus pH for papain have been attributed to the imidazolium−thiolate ionic pair of the conserved active-site His and Cys residues (*13–21*). As the p*K* values found in the plots of log k_{cat}/K_a versus pH for cathepsin C likely describe enzymatic residues on the free enzyme form, we tentatively assign the enzymatic groups with a pK_1 of 4.3 and a pK_2 of 6.5 to Cys-234 and His-381, respectively, while the identity of the enzymatic group that constitutes the pK_3 of 7.7 is unknown.

The plot of log k_{cat} versus pH similarly conformed to a classic bell-shaped curve, in which log k_{cat} decreased at both acidic and basic pH values with asymptotic slopes of 1 and −1, respectively (Figure 1 and Table 1). For the plot of log k_{cat} versus pH, the enzymatic group with a pK_5 of 7.7 could represent His-381, which would be expected to be more basic in the complexes from EX to FX (complexes which likely define the k_{cat} expression) than in enzyme forms E and EA in Scheme 1, since Cys-234 is not available for formation of a hydrogen bond to His-381 in the latter complexes. Cathepsin C contains a unique structural feature in that its N-terminal residue, Asp-1, is part of an exclusion domain of the protein in which its β-carboxylic side chain apparently contributes to the recognition of N-terminal dipeptide substrates by establishing an ion pair with the N-terminal amino group of substrates such as SY-AMC (*44*). It is therefore possible that pK_4, which does not appear in the plot of log k_{cat}/K_a versus pH, represents the carboxylic side chain of Asp-1 such that protonation below pH 3.5 renders it unable to form this complex with the N-terminal amino group of the substrate, as reflected in the observed pH−rate profile for k_{cat}.

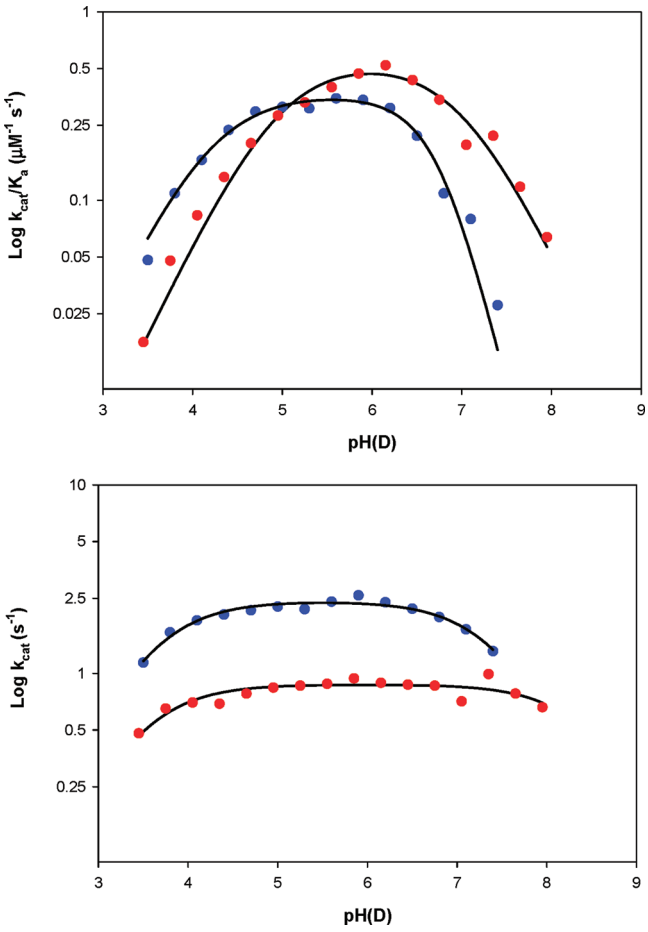

FIGURE 1: pH−rate profiles of log k_{cat}/K_a (top panel) and log k_{cat} (bottom panel) vs pH (blue) and pD (red) for cathepsin C using SY-AMC as a substrate. The lines drawn through the experimental points represent the fitting to eq 2 for all plots except the plot of log k_{cat}/K_a vs pH, which was fitted to eq 3. Fitting results are found in Table 1. Experimental conditions and details may be found in Experimental Procedures.

Steady-State Kinetics of Cathepsin C: Solvent Kinetic Isotope Effects. sKIEs on cathepsin C with SY-AMC were obtained from plots of log k_{cat}/K_a and log k_{cat} in solutions composed of 93.5% D_2O, as shown in Figure 1. As in the case of the pH−rate profile, the plot of log k_{cat}/K_a versus pD was described by a bell-shaped curve, in which apparent slopes at acidic and basic pH were 1 and −1, respectively (Figure 1 and Table 1). An inverse sKIE was observed on k_{cat}/K_a [$^D(k_{cat}/K_a) = 0.71 \pm 0.14$].[3] The p$K$ values pK_1 and pK_2 in D_2O shifted from the H_2O values by +0.6 and +0.4 unit, respectively, and may result from the solvent equilibrium isotope effect on the catalytic residues attributed to these pK values. Since the solvent equilibrium isotope effects on the pK values (ΔpK) on sulfhydryl and histidinyl groups are typically 0.15−0.18 and 0.5−0.7, respectively (*33*), it is not possible to assign either of the two pK values unambiguously to either the His-381 or Cys-234. It is unclear why the group defined by pK_3 (7.7 in H_2O) is not observed in the plot of log k_{cat}/K_a versus pD, except to suggest that the enzymatic group responsible for this pK value remains deuteriated at the upper value of pD used in this study, due to the expected increase in the value of pK_3 in D_2O. As in H_2O, a classical bell-shaped curve was observed for the plot of log k_{cat} versus pD (Figure 1 and Table 1), with pK values similar to those found in H_2O, and a normal sKIE on k_{cat} was observed ($^Dk_{cat} = 2.76 \pm 0.04$).

Interestingly, the pH/pD profiles of cathepsin C displayed an inverse sKIE on k_{cat}/K_a but a normal sKIE on k_{cat}. This result immediately suggested that the kinetic parameters k_{cat}/K_a and k_{cat} encompass distinct catalytic steps in cathepsin C separated by an irreversible step, such as the release of AMC product following acylation of the enzyme (Scheme 1). While the $^D(k_{cat}/K_a)$ parameter contains only kinetic steps for the acylation half-reaction and these steps could express both an inverse sKIE and a normal sKIE, the $^Dk_{cat}$ parameter contains kinetic steps of both half-reactions, of which the deacylation half-reaction would be expected to express only normal sKIEs. Inverse sKIEs have been demonstrated for the acylation half-reaction of papain using benzyl-argininamide [$^Dk = 0.58$ (*14*)] and carbobenzoxycarbonyl-phenylalanyl-glycinamide [$^Dk = 0.63$ (*14*)] and in covalent inactivation studies (*15–20*). As described in the theory section, the inverse sKIE on the $^D(k_{cat}/K_a)$ expression likely arises from an enrichment of the E tautomer in D_2O, which contains the active thiolate−imidazolium forms of Cys-234 and His-381. The thiolate−imidazolium tautomer of the free enzyme form (E) of cathepsin C will be enriched in D_2O by the ratio $[E]_{H_2O}/[E]_{D_2O} = (1 + K_{t1}/^DK_t)/(1 + K_{t1})$. From a ^DK_t of 2.56 (*33, 36*) and the estimate for K_{t1} of 0.7 from this work, the $[E]_{H_2O}/[E]_{D_2O}$ ratio may be calculated to be 0.75, which is nearly equal to the observed inverse value of 0.71 for $^D(k_{cat}/K_a)$. From this, the active tautomer of cathepsin C will be 34% more abundant in D_2O than H_2O. The increased amount of E in D_2O apparently offsets any expression of the expected normal sKIE from the k_5 step on the $^D(k_{cat}/K_a)$ parameter (eq 14). Also, for a K_{t1} of 0.7, one may calculate a ratio for the thiolate−imidazolium:thiol−imidazole tautomers (E:E′) of 1.5:1 from the relationship $f_1 = [E]/([E'] + [E]) = 0.6$, which is in accord with previous reports (*15–18*).

Transient Kinetics of Cathepsin C. Pre-steady-state time courses (2−200 ms) for the cathepsin C reaction with fixed concentrations of SY-AMC (4−30 μM) were obtained in both H_2O and D_2O (Figure 2 and Table 2). As exemplified by the time course generated from 5 μM substrate in Figure 2, time courses for all substrate concentrations in both solvents were described by a rapid burst of AMC formation followed by a steady-state linear rate of product formation. We found at substrate concentrations of <4 μM transient kinetic data fit better to a double-exponential expression (eq 7), whereas at all higher substrate concentrations, data fit better to a single-exponential expression (eqs 6 and 8) (F-test, $p > 0.05$). These results suggested that at ≥4 μM SY-AMC, the second exponential term, containing the exponential rate constant λ_2 as found in eqs 7, 25, and 27, becomes vanishingly small and no longer contributes to the transient kinetic rates.

At all substrate concentrations, the time courses obtained appeared to demonstrate faster transient bursts (when $t \leq 60$ ms) and steady-state ($t \geq 60$ ms) rates in H_2O than in

[3] To evaluate whether the respective inverse and normal sKIEs observed on k_{cat}/K_a and k_{cat} for cathepsin C were due to the effects of solvent viscosity imparted by 93.5% D_2O, we measured these values in 0−12% (w/v) glycerol ($\eta_{rel} = 1.0-1.28$) as described previously (*45*). At glycerol concentrations equivalent to the solution viscocity of 93.5% D_2O, k_{cat}/K_a decreased by 29% and k_{cat} increased by 17%, effects which are opposite from those observed in D_2O, thereby indicating that the measured sKIEs did not arise from changes in solvent viscosity.

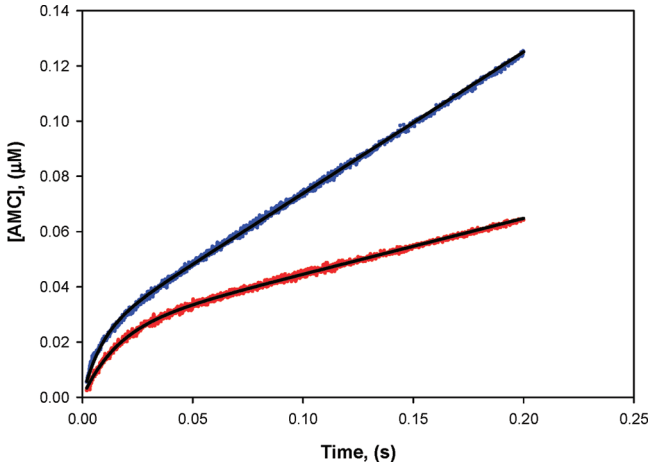

FIGURE 2: Pre-steady-state time courses of cathepsin C (0.046−0.051 μM) in H_2O (blue curves) and D_2O (red curves) [pH(D) 5.6] using a final SY-AMC concentration of 5 μM. The lines drawn through the experimental points represent the fits to eq 6, yielding the following values: $k_{ss} = 0.51$ μM/s, $\beta = 0.023$ μM, and $\lambda = 120 \pm 0.40$ s^{-1} in H_2O, and $k_{ss} = 0.20$ μM/s, $\beta = 0.024$ μM, and $\lambda = 64 \pm 0.17$ s^{-1} in D_2O. Experimental conditions and details may be found in Experimental Procedures.

D_2O, indicating that normal solvent isotope effects were present on the transient kinetics. Accordingly, time courses in both H_2O and D_2O for each fixed substrate concentration from 5 to 30 μM were fitted to the single-exponential function in eq 6 (F-test, $p > 0.05$). The kinetic parameters derived from these individual fits were the steady-state rate, k_{ss}, the burst amplitude, β, and the transient burst rate, λ. All three parameters were replotted versus the substrate concentration (Figure 3).

The replot of the steady-state rate, k_{ss}, versus [A], as shown in Figure 3A, was well-fitted to the hyperbolic function of eq 29, which resulted in the following values: $k_{cat} = 17.1 \pm 0.09$ s^{-1} and $K_{a'} = 2.06 \pm 0.05$ μM in H_2O, and $k_{cat} = 6.37 \pm 0.09$ s^{-1} and $K_{a'} = 1.4 \pm 0.1$ μM in D_2O. This replot fit indicated that a normal sKIE of 2.7 exists on the steady-state rate (k_{ss}), identical to that determined from the steady-state sKIE from pH(D) plots ($^{D}k_{cat} = 2.76 \pm 0.04$), while the $K_{a'}$ value is slightly lower in D_2O than in H_2O. The replots of the burst rate (λ) vs [A] were fitted to eq 31, for which a normal sKIE of 1.5 was observed on the burst rate: $k_{ac} = 380 \pm 21$ s^{-1} in H_2O, and $k_{ac} = 290 \pm 27$ s^{-1} in D_2O (Figure 3B). The replot of the amplitude of the burst rate (β) vs [A] (Figure 3C) revealed that the maximal burst amplitude at high substrate concentrations corresponded to 0.045 μM AMC product, which is nearly equal to the active-site concentrations of cathepsin C (0.046−0.05 μM) used in these studies.

Interestingly, the burst amplitude and its concentration dependence at all substrate concentrations are approximately the same in D_2O and H_2O, suggesting that the different distributions of the tautomeric enzyme forms in the two solvents are ablated by rapid turnover and re-equilibration of the preferred tautomers E and EA as they are converted into downstream species in the transient phase. Additionally, the lack of a sKIE on the burst amplitude is evident from eq 32, since under the conditions of these experiments where $k_{ac} \gg k_{dac}$, there would be no isotope-dependent terms remaining in this expression (eq 32). In summary, while a normal sKIE was observed on the steady-state portion of the time courses, no inverse sKIE was observed in the transient data, and a normal sKIE of ~1.5 (on the burst rate) was observed which could not be detected by the steady-state studies. Since eq 8 relates transient product formation observed in the time courses to several kinetic parameters that cannot be solved by these standard replot analyses, a global fitting procedure was carried out.

We fitted all transient rate data for all concentrations of SY-AMC (5−30 μM), in both H_2O and D_2O. For each solvent, approximately 200000 data points were fitted to eq 8, with results listed in Table 2. The full set of kinetic parameters k_{cat}, k_{ac}, k_{dac}, $K_{a'}$, and K_{ia1} were all well-determined by the global fitting procedure, as opposed to the partial set obtained from the standard replots method as depicted in Figure 3. The determined k_{ac} value of 397 ± 5 s^{-1} in H_2O was much larger than the nearly identical values of k_{dac} (13.95 ± 0.01 s^{-1}) and k_{cat} (13.92 ± 0.001 s^{-1}), confirming that the deacylation half-reaction of cathepsin C comprises the rate-limiting component of the mechanism. Also, the fitted results are self-consistent since calculation of k_{cat} from these derived values of k_{ac} and k_{dac}, from $k_{cat} = k_{ac}k_{dac}/(k_{ac} + k_{dac})$, yields a value of 13.5 s^{-1}, which is nearly identical to the experimentally determined value (13.92 ± 0.001 s^{-1}). In H_2O, the pseudo-Michaelis constant ($K_{a'} = 1.75 \pm 0.003$ μM) was considerably smaller than the steady-state Michaelis constant ($K_a = 6.9 \pm 0.2$ μM), which can occur when rapid equilibrium conditions do not strictly apply (i.e., in eq 12, when the a, b, and/or c values are non-zero). In D_2O, rate constants obtained from the global fit were proportionately lower than those obtained from H_2O: $k_{ac} = 308 \pm 3$ s^{-1}, $k_{dac} = 5.27 \pm 0.009$ s^{-1}, and $k_{cat} = 5.26 \pm 0.008$ s^{-1}, yet the substrate dissociation constant ($K_{ia1} = 15.2 \pm 0.25$ μM) in D_2O was larger than the H_2O value. A comprehensive interpretation of these kinetic parameters determined by global fitting could now be attained through calculation and evaluation of the apparent sKIEs on all of these parameters (Table 2), as described in the next section.

Solvent Kinetic Isotope Effects from the Transient Kinetics. sKIEs were determined for k_{cat}, k_{dac}, k_{ac}, $K_{a'}$, and K_{ia1} from ratios of the values in Table 2 as obtained in the two solvents: $^{D}k_{ac} = 1.31 \pm 0.04$, $^{D}k_{dac} = 2.76 \pm 0.03$, $^{D}K_{a'} = 1.15 \pm 0.02$, and $^{D}K_{ia1} = 0.68 \pm 0.03$, which may be compared to the steady-state values of $^{D}(k_{cat}/K_a) = 0.71 \pm 0.14$ and $^{D}k_{cat} = 2.76 \pm 0.04$. Like the equality of the k_{cat} and k_{dac} values, the steady-state and transient values of $^{D}k_{cat}$ are also nearly identical to that of $^{D}k_{dac}$, which further supports the proposal that the deacylation half-reaction is rate-limiting for the cathepsin C reaction pathway and that the kinetic steps and rate constants of the acylation half-reaction make little contribution to the k_{cat} and $^{D}k_{cat}$ terms.

The $^{D}k_{ac}$ value of 1.31 ± 0.04 reflects the sKIE for the acylation half-reaction of cathepsin C. As noted above, normal sKIEs were observed for the transient rates at all substrate concentrations from 1 to 30 μM. The normal isotope effect on $^{D}k_{ac}$ stands in contrast to the inverse isotope effect on the steady-state $^{D}(k_{cat}/K_a)$ value of 0.71, which also contains the kinetic steps of the acylation half-reaction. Contributions to the value of the sKIE for $^{D}(k_{cat}/K_a)$ arise from two sources: (1) an expected normal kinetic isotope effect on the k_5 step of the acylation half-reaction and (2) the inverse kinetic isotope effect expected from the solvent equilibrium isotope effect which enriches the distribution of

Table 2: Transient Rate Kinetics of Cathepsin C in H_2O and D_2O [pH(D) 5.6][a]

solvent	k_{cat} (s^{-1})[b]	k_{ac} (s^{-1})	k_{dac} (s^{-1})	$K_{a'}$ (μM)[b]	K_{ia1} (μM)
H_2O	13.92 ± 0.001	397 ± 5	13.95 ± 0.013	1.75 ± 0.003	10.4 ± 0.3
D_2O	5.26 ± 0.008	308 ± 3	5.27 ± 0.009	1.53 ± 0.003	15.2 ± 0.25

	$^{D}k_{cat}$	$^{D}k_{ac}$	$^{D}k_{dac}$	$^{D}K_{a'}$	$^{D}K_{ia1}$	tKIE°
sKIE[c,d]	2.76 ± 0.04	1.31 ± 0.04	2.76 ± 0.03	1.15 ± 0.02	0.68 ± 0.03	2.3 ± 0.2

[a] Transient rate data of product vs time for 5−30 μM SY-AMC in both H_2O and D_2O were fitted for each solvent to eq 8 for E_t values of 0.046 and 0.051 μM in H_2O and D_2O, respectively. [b] By comparison to its steady-state counterpart values in Table 1, a k_{cat} of 13.92 ± 0.001 s^{-1} and a $k_{cat}/K_{a'}$ of 7.96 ± 0.002 μM^{-1} s^{-1}, determined from transient kinetics, were much larger, in part because of the observed effect at concentrations of cathepsin C greater than 1 nM, an observed unexplained increase in k_{cat} and k_{cat}/K_a (6- and 20-fold, respectively), than that seen at 10−20 pM. [c] Apparent sKIEs were calculated from the fitted transient kinetic parameters using eq 4, and the error was determined using eq 5. [d] The transient kinetic isotope effect was obtained by determining the sKIE at 5, 7.5, 17.5, and 20 μM SY-AMC for data at 2−60 ms as shown in Figure 4, and extrapolating back to time zero. The value is the average of the four concentrations.

the active E tautomer in D_2O. Assuming that the E and E′ tautomers are rapidly re-equilibrated after conversion of E to EA in either solvent, much faster than the sampling time of the transient kinetics, inverse solvent kinetic isotope effects were not evident in the transient kinetics.

The expression for $^{D}k_{ac}$ (eq 18) contains the term $K_{t2}/^{D}K_t$ in its numerator, which reflects the fact that the concentration of EA in D_2O is greater than in H_2O (or, $[EA]_{D_2O}/[EA]_{H_2O} > 1$), which would contribute an inverse solvent equilibrium isotope effect in the measured $^{D}k_{ac}$ parameter. That $^{D}k_{ac}$ is a normal solvent isotope effect of 1.31 indicates that the value of $^{D}k_5$ compensates for or overwhelms any contribution of the $K_{t2}/^{D}K_t$ term in the $^{D}k_{ac}$ expression.

The $^{D}K_{ia1}$ value of 0.68 ± 0.03 is unusual since solvent isotope effects on a substrate dissociation constant are normally unexpected. From Scheme 1 and eq 12, the expression for $^{D}K_{ia1}$ may be written as eq 36.

$$^{D}K_{ia1} = [(1 + K_{t2}/^{D}K_t)(1 + K_{t1})]/[(1 + K_{t1}/^{D}K_t)(1 + K_{t2})] \quad (36)$$

If the enzyme forms E and EA are enriched in D_2O to different extents, that is [EA]/[E′A] < [E]/[E′] or $K_{t2} > K_{t1}$, then the value of $^{D}K_{ia1}$ may be expected to be <1.

Next, we used the methodology of Palfey and Kagan (*39*) and Maniscolo et al. (*40*) to evaluate the kinetic isotope effect of the transient phase (tKIE) extrapolated to time zero (tKIE°). As described in the theory section, the limiting value of the tKIE, tKIE°, is a function of the intrinsic isotope effect on the k_5 step and the solvent equilibrium isotope effect on the concentration of the E tautomer (eq 35). Shown in Figure 4 are experimental values of tKIE, calculated by dividing the time course data obtained in H_2O by that obtained in D_2O, for the data shown in Figure 2 (5 μM substrate) at $t \leq$ 60 ms. It is clear that as time increases from 0 to >10 ms, values of tKIE decrease from >2.0 to a value equivalent to that of $^{D}k_{ac}$ (1.3−1.4). The average value of tKIE° at four different substrate concentrations was 2.3 ± 0.2. The observation that an apparent intrinsic solvent kinetic isotope effect of 2.3 diminishes to a value of 1.3−1.4 as time progresses in the transient phase suggests that a slow kinetic step follows the isotope sensitive one, k_5. This is evident when one examines the expressions for $^{D}k_{ac}$ (eq 18) and tKIE° (eq 35), in that the former expression contains the k_7 rate constant while the latter does not. In the case where the rate of desorption of AMC from the FP complex is equal to or slower than its rate of formation ($k_7 \leq k_5$), at $t >$ 10 ms, and as the EX complex progresses to the FP complex, a low value for k_7 will lead to EX achieving its steady-state concentration during the transient phase. Under these conditions, the expression of the intrinsic solvent isotope effect $^{D}k_5$ will be attenuated by the k_7 step as FP accumulates and EX and FP come to equilibrium, whereupon the intrinsic kinetic isotope effect $^{D}k_5$ is replaced by its lower equilibrium value $^{D}K_{eq5}$, which is nearly equal to unity.

Determination of the Individual Kinetic Constants from the Steady-State and Pre-Steady-State Kinetics of Cathepsin C. From the 12 measured kinetic parameters acquired for cathepsin C under pre-steady-state and steady-state conditions summarized in Table 3, one may now produce at least one set of self-consistent values of the intrinsic kinetic and equilibrium isotope effects, ratios of the individual rate constants, approximation of individual rate constants, and the ratios of the tautomeric forms of the enzyme (K_{t1} and K_{t2}) for the chemical mechanism in Scheme 1. Assuming that the commitment factor $k_6/k_7 = c = 0$ and employing literature values of fractionation factors ($^{D}K_t = 2.56$, $^{D}K_{eq5} = 0.91$, $^{D}K_{eq9} = 0.86$, and $^{D}K_{eq11} = 2.79$) (*36, 46*), we used SAS to simultaneously solve the 12 equations describing all values of intrinsic isotope effects, commitment factors, and equilibrium constants, using the experimental values derived in this work so far.

Listed in Table 3 are the results of these fittings, from which the individual rate constants for the kinetic steps in Scheme 1 were solved or approximated from the commitment factors obtained from the simultaneous fittings. As a verification of these fittings, we reinserted the solved intrinsic values and individual rate constants into the 12 equations and calculated values for the 12 kinetic parameters (Table 3, calculated value), for comparison with their experimental counterparts. All calculated values are within 5% of their experimental values.[4] The solved values of the intrinsic kinetic and equilibrium isotope effects are all reasonable with the potential exception of the K_{t2} of 4.9, which indicates that the thiol−imidazole tautomer (E′A) of the Cys-His dyad is highly favored in the substrate-bound enzyme form. In contrast, for the free enzyme, the K_{t1} value of 0.7 indicates that the amount of the thiolate−imidazolium (E) tautomer exceeds that of the thiol−imidazole (E′) form by 1.5-fold,

[4] Calculation of k_{ac-ss} from eq 13a using the values in Table 3 results in a value of 155 s^{-1}, which differs from the transient rate (k_{ac} = 397 s^{-1}). The lack of agreement can be attributed to the value of the commitment factor b (k_5/k_4), which was found in this work to be greater than zero (b = 220). Under strict rapid equilibrium conditions where b equals zero, k_{ac-ss} would equal k_{ac} (eq 17).

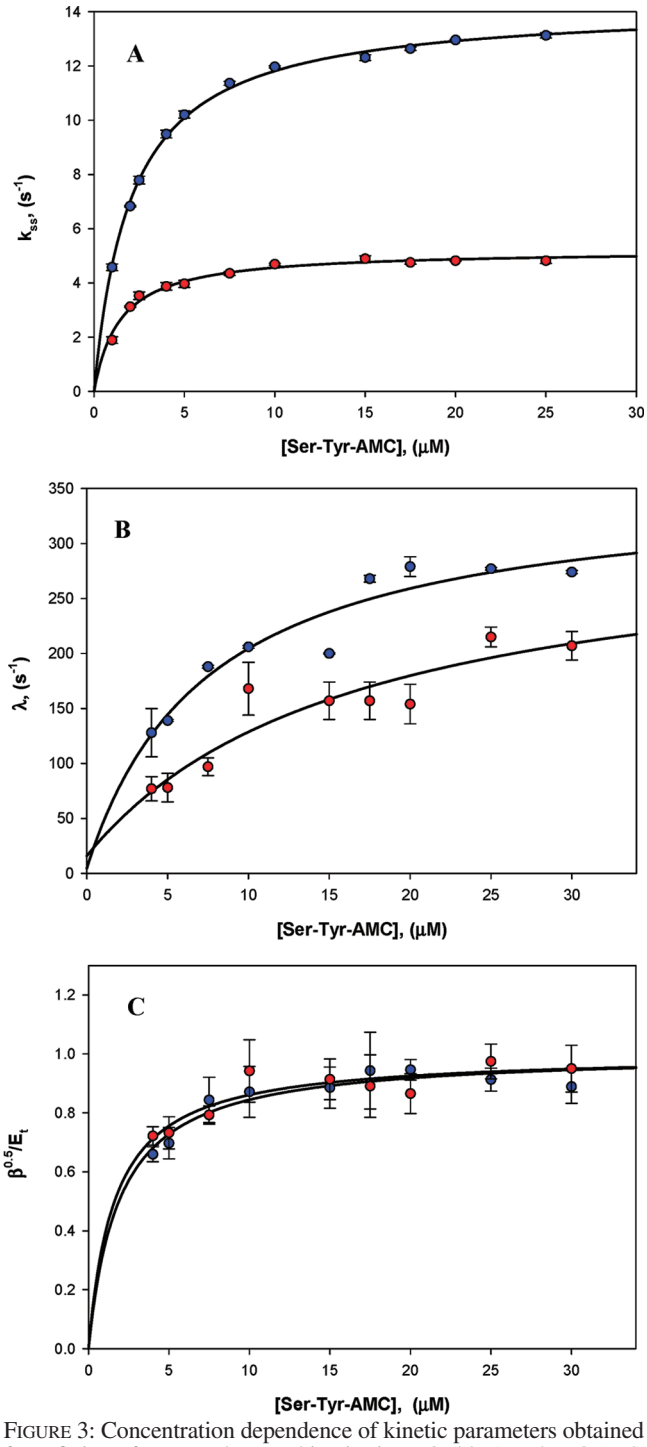

FIGURE 3: Concentration dependence of kinetic parameters obtained from fitting of pre-steady-state kinetics in H_2O (blue) and D_2O (red) [pH(D) 5.6] to eq 6. (A) Replot of the steady-state rate (k_{ss}) vs [Ser-Tyr-AMC]. The black curves drawn through the experimental points (average of three determinations) represent fitting the data to eq 29, resulting in the following values: $k_{cat} = 17 \pm 0.1\ s^{-1}$ and $K_{a'} = 2.1 \pm 0.05\ \mu M$ in H_2O, and $k_{cat} = 6.4 \pm 0.1\ s^{-1}$ and $K_{a'} = 1.4 \pm 0.1\ \mu M$ in D_2O. (B) Replots of the pre-steady-state transient rate (λ) vs [Ser-Tyr-AMC]. The curves drawn through the experimental points (average of three determinations) were obtained by fitting the data to eq 31, resulting in the following values: $k_{ac} = 380 \pm 21\ s^{-1}$, $k_{dac} = 1 \pm 19\ s^{-1}$, and $K_{ia1} = 9 \pm 3\ \mu M$ in H_2O, and $k_{ac} = 290 \pm 27\ s^{-1}$, $k_{dac} = 1 \pm 13\ s^{-1}$, and $K_{ia1} = 13 \pm 4\ \mu M$ in D_2O. (C) Replots of the square root of the burst amplitude (β) vs [SY-AMC]. The curves drawn through the experimental points (average of three determinations) were obtained by fitting the data to eq 32, resulting in $K_{a'}$ values of $1.91 \pm 0.37\ \mu M$ in H_2O and $1.6 \pm 0.41\ \mu M$ in D_2O. Experimental conditions and details may be found in Experimental Procedures.

which is more in accord with experimental data for other cysteine proteases (*15–18*). Under our experimental conditions, lowering the solution dielectric constant via the presence of 5% DMSO may contribute to an apparent increase in the proportion of the neutral forms of the Cys-His dyad over that of their ionic counterparts.

As an additional verification of the solutions to the individual rate constants and intrinsic isotope effects of the chemical mechanism of cathepsin C found in Table 3, we used simulation software (see Experimental Procedures) and the mechanism shown in Scheme 1 to create simulated time courses of the transient kinetics in both H_2O and D_2O to compare with the experimental data. For these simulations, the observed fluorescence signal was assumed to arise from the EX, FP, and P species,[2] and the simulated time courses were constructed from the solved rate constants k_1-k_{13} summarized in Table 3. For simulations of the time courses in D_2O, the isotope-sensitive rate constants k_1, k_5, k_9, k_{10}, and k_{11} were calculated as follows: $k_{1D_2O} = k_{1H_2O}{}^{D}K_{ia1}$, $k_{5D_2O} = k_{5H_2O}/{}^{D}k_5$, $k_{9D_2O} = k_{9H_2O}/{}^{D}k_9$, $k_{10D_2O} = k_{10H_2O}{}^{D}K_{eq9}/{}^{D}k_9$, and $k_{11D_2O} = k_{11H_2O}/{}^{D}k_{11}$. The time courses simulated in either solvent superimposed on the experimental data remarkably well (see Figure 5 for 5 and 20 μM substrate time course examples), thereby indicating that the set of solved rate constants and intrinsic isotope effects is consistent with the experimental data.

The full set of kinetic values derived from this work also allowed estimation through simulation of the kinetic profile in Scheme 1 of the levels of all enzyme forms during catalysis. As shown in Figure 6, during steady-state catalysis, cathepsin C exists primarily (~80%) in the acylated form, F (43%) or FX (33%). The current crux of drug discovery for cysteine and serine proteases is that inhibitors act primarily through reaction with the active-site cysteine. Our results suggest that in the presence of substrate, the enzyme becomes primarily acylated and potentially more available to bind inhibitors synergistically or noncompetitively with substrate, thereby bypassing the cysteine reactivity problems. We may now have another strategy for screening for and/or rational design of more efficacious inhibitors via probing the acylated form of the enzyme.

Chemical Mechanism of Cathepsin C. The chemical mechanism that this work proposes for cathepsin C, that of Scheme 1, not only confirms many of the features derived from previous studies on other cysteine proteases (*13–22*) but also expands on the previous knowledge by providing relative rates of several steps during catalysis. As we have now shown, for the SY-AMC substrate, the acylation half-reaction is much more rapid than its deacylation counterpart such that k_{cat} is completely constrained by its component half-reaction, k_{dac}. The pH−rate data reported in this study are inconclusive in terms of the definitive assignment of the enzymatic groups of pK values of 4.3 and 6.7 to His-381 and Cys-234, respectively, but these values are completely consistent with those observed for the active-site histidinyl and cysteinyl residues of other cysteine proteases. At the pH optimum, the thiolate form of Cys-234 and the imidazolium form of His-384 are 1.5-fold more abundant than their neutral counterparts ([E] > [E′]), so the observed inverse value of ${}^{D}(k_{cat}/K_a)$ arises entirely from the enrichment in D_2O of tautomeric form E. That is, contrary to some reports that inverse effects are due to kinetic or substrate-induced

Table 3: Summary of the Kinetic Parameters, Solved Commitment Factors, Intrinsic Isotope Effects, and Individual Rate Constants for Cathepsin C[a]

equation number	kinetic parameter	experimental value	calculated value	solved intrinsic isotope effects, commitment factors, and tautomer constants	calculated individual rate constants
11	k_{cat}/K_aE_t	$7.95 \pm 0.002\ \mu M^{-1}\ s^{-1}$	$7.4\ \mu M^{-1}\ s^{-1}$	$^Dk_5 = 3.2$	$k_1 \cong 18\ \mu M^{-1}\ s^{-1}$
33	K_{ia1}	$10.4 \pm 0.3\ \mu M$	$10.4\ \mu M$	$^Dk_9 = 2.6$	$k_2 \cong 650\ s^{-1}$
14	$^D(k_{cat}/K_a)$	0.71 ± 0.14	0.74	$^Dk_{11} = 3.2$	$k_3 \cong 1500\ s^{-1}$
17	k_{ac}/E_t	$397 \pm 5\ s^{-1}$	$397\ s^{-1}$	$k_3/k_2 = 2.3$	$k_4 \cong 13\ s^{-1}$
18	$^Dk_{ac}$	1.31 ± 0.04	1.31	$k_5/k_4 = 220$	$k_5 \cong 2900\ s^{-1}$
13b	k_{dac}/E_t	$13.95 \pm 0.001\ s^{-1}$	$14.4\ s^{-1}$	$k_6/k_7 \sim 0$	$k_6 \cong 0.1$
16	$^Dk_{dac}$	2.76 ± 0.03	2.84	$k_3/k_5 = 0.5$	$k_7 \cong 460\ s^{-1}$
10	k_{cat}/E_t	$13.92 \pm 0.001\ s^{-1}$	$13.2\ s^{-1}$	$k_5/k_7 = 6.2$	$k_9 \cong 115\ s^{-1}$
15	$^Dk_{cat}$	2.76 ± 0.04	2.67	$k_{10}/k_{11} = 2.8$	$k_{10} \cong 100\ s^{-1}$
35	tKIE°	2.3 ± 0.3	2.4	$k_{12}/k_{13} \sim 0.15$	$k_{11} \cong 36\ s^{-1}$
30	$K_{a'}$	$1.75 \pm 0.003\ \mu M$	$1.7\ \mu M$	$k_9/k_{11} = 3.2$	$k_{12} < 150\ s^{-1}$
36	$^DK_{ia1}$	0.68 ± 0.03	0.65	$k_{11}/k_{13} < 0.1$	$k_{13} > 1000\ s^{-1}$
				$k_3 = 1500\ s^{-1}$	
				$k_9 = 115\ s^{-1}$	
				$K_{t1} = 0.7$	
				$K_{t2} = 4.9$	

[a] Experimental kinetic parameters are those found in this work and reported in Tables 1 and 2. Solved values were obtained from simultaneous solution of the 12 equations in column 1 using the experimental values in column 3, fixed (literature) values for ^DK_t (2.56), $^DK_{eq5}$ (0.91), $^DK_{eq9}$ (0.86), and $^DK_{eq11}$ (2.79), and the solved ratios of rate constants for the kinetic steps in Scheme 1 (*36, 46*). Individual rate constants were then derived by starting with values for k_3 and k_9 that were solved by the fitting, and then calculating the rest of the rate constants on the basis of the solved ratios (commitment factors), listed in column 5. The rate constant values listed in column 6 are not exact but represent ranges (within ~5%) of numbers that are consistent with all fitting routines carried out in this work.

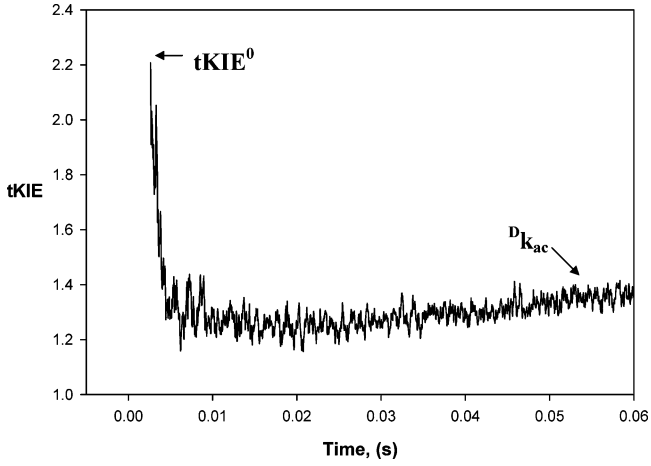

FIGURE 4: Transient kinetic isotope effects for cathepsin C. tKIE was determined by division of the [AMC] at each time point from 0.002 to 0.060 s in H_2O by the corresponding value in D_2O at 5 μM substrate. Experimental conditions and details may be found in Experimental Procedures.

formation of the thiolate−imidazolium pair, the setting up of this catalytically competent form of the enzyme is not a kinetic but an equilibrium step.

This work also provides estimates of the rate constants and intrinsic solvent isotope effects for the individual reaction steps. The solved values in Table 3 suggest that the conversions of E to EA to EX are highly committed kinetic steps ($k_3/k_2 = 2.3$, $K_{eq3} = 115$, and $k_5/k_4 = 222$), which is reflected in the large experimental value for the transient rate of acylation ($k_{ac} = 397\ s^{-1}$). For the acylation half-reaction, the solved values of k_3 ($1500\ s^{-1}$), k_4 ($13\ s^{-1}$), and K_{eq3} (115) indicate that as expected the attack of the active-site thiolate in EA on the substrate to form the tetrahedral intermediate in the EX complex is heavily favored kinetically and thermodynamically, and likewise, the collapse of this tetrahedral intermediate to form the acylated enzyme−product form FP is also a strongly committed step ($k_5 = 2900\ s^{-1}$ and $k_6 \sim 0$). This is also reflected in the time course simulations (Figure 6B), for which both [EA] and [EX] rise and fall at very low time points in the transient phase. The conversion of the EX intermediate to the FP complex involves protonation of the scissile AMC group by the imidazolium on His-384, which would constitute the normal solvent isotope effect calculated as $^Dk_5 = 3.2$ (Table 3). A normal solvent isotope effect would be expected in the chemical step in which the tetrahedral intermediate in EX is converted to the acylated form of cathepsin C, FP, as it involves one primary and two secondary hydrogen isotope effects. That the simulated time course of the formation and conversion of the enzyme species EX in Figure 6 is very rapid suggests that the acylation half-reaction of cathepsin C, using SY-AMC as a substrate, involves a fleeting tetrahedral intermediate, and accordingly, the conversion of EA to FP is a nearly concerted reaction. Previous analyses of the heavy atom kinetic isotope effects of papain using *p*-nitrophenyl acetate as a substrate (labeled in the carbon and oxygen atoms of the carbonyl group and the phenolate oxygen atom) have shown that the acylation half-reaction proceeds via a concerted mechanism (*48*). Our finding that a short-lived tetrahedral intermediate exists in the acylation half-reaction of cathepsin C is consistent with these results in that the *p*-nitrophenolate is expected to be a better leaving group than the aminocoumarin group of SY-AMC. Moreover, unlike that of *p*-nitrophenolate, departure of the aminocoumarin group of AMC requires protonation by the imidazolium species, which would favor the existence of a tetrahedral intermediate.

Interestingly, our results indicate that the desorption of the AMC product from the FP complex is sufficiently slow ($k_7 = 460\ s^{-1}$) that it could be the rate-limiting step of the acylation half-reaction, as seen in the increase in FP concentration in the transient phase in panels A and B of Figure 6. The relatively low k_7 value of $460\ s^{-1}$ results in FP concentration being the predominant species during the transient phase of acylation in either solvent, although in D_2O the sKIE on the k_5 step leads to an increased EX concentration and a decreased FP concentration compared to those in H_2O (Figure 6C). This suggests that the bicyclic

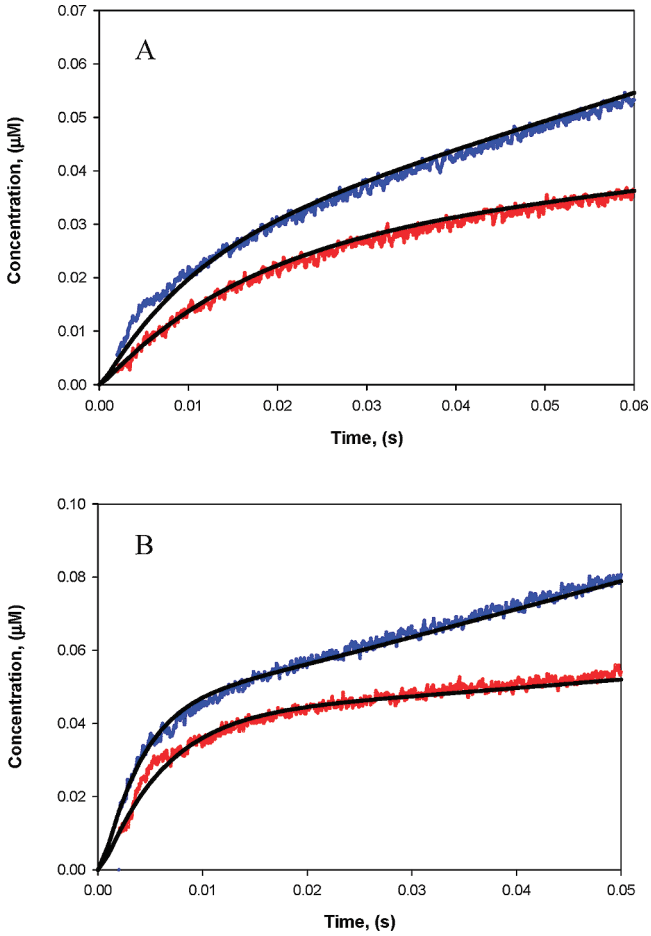

FIGURE 5: Simulations of time courses of the transient kinetics of cathepsin C in H_2O and D_2O. Experimental data are shown in blue for H_2O and red for D_2O, where the concentration represents the concentration of AMC as determined by quantification of the fluorescence signal. Simulations are shown in solid black lines, where the concentration represents the sum of the concentrations of EX, FP, and P. Simulations were generated by using the mechanism outlined in Scheme 1 and the rate constants k_1-k_{13} listed in Table 3. The rate constants used for the D_2O simulations were calculated on the basis of the sKIEs on some of these steps (see the text for clarification): $k_1 = 12\ \mu M^{-1}\ s^{-1}$, $k_2 = 648\ s^{-1}$, $k_3 = 1500\ s^{-1}$, $k_4 = 13\ s^{-1}$, $k_5 = 900\ s^{-1}$, $k_6 = 0.03\ s^{-1}$, $k_7 = 464\ s^{-1}$, $k_9 = 44\ s^{-1}$, $k_{10} = 34\ s^{-1}$, $k_{11} = 12\ s^{-1}$, $k_{12} = 0.1\ s^{-1}$, and $k_{13} = 10000\ s^{-1}$. (A) Time course simulations and data for 5 μM substrate and 42 nM enzyme. (B) Time course simulations and data for 20 μM substrate and 52 nM enzyme.

aromatic moiety of the AMC product may render it "sticky" in the enzyme active site, which lends support to the notion that finding inhibitors that bind to the acylated form of the enzyme is possible. That k_7 is smaller than k_5 further substantiates the reason why the apparent value of tKIE decreases from 2.3 at $t \rightarrow 0$ to 1.3 at $t > 10$ ms, since at longer reaction times in D_2O, the effect of $^{D}k_5$ on tKIE is attenuated as the EX and FP complexes nearly come to equilibrium. This is also shown in the early part of the transient in D_2O, shown in Figure 6C, as the "peak concentration" of EX increases and broadens while the peak FP concentration diminishes and broadens compared to the H_2O transient data in Figure 6B.

In the deacylation half-reaction, the unprotonated His-381 likely represents the group corresponding to the measured pK of 7.7 in the pH−rate profile of k_{cat} and acts as a general base to remove the proton on the lytic water. The solved

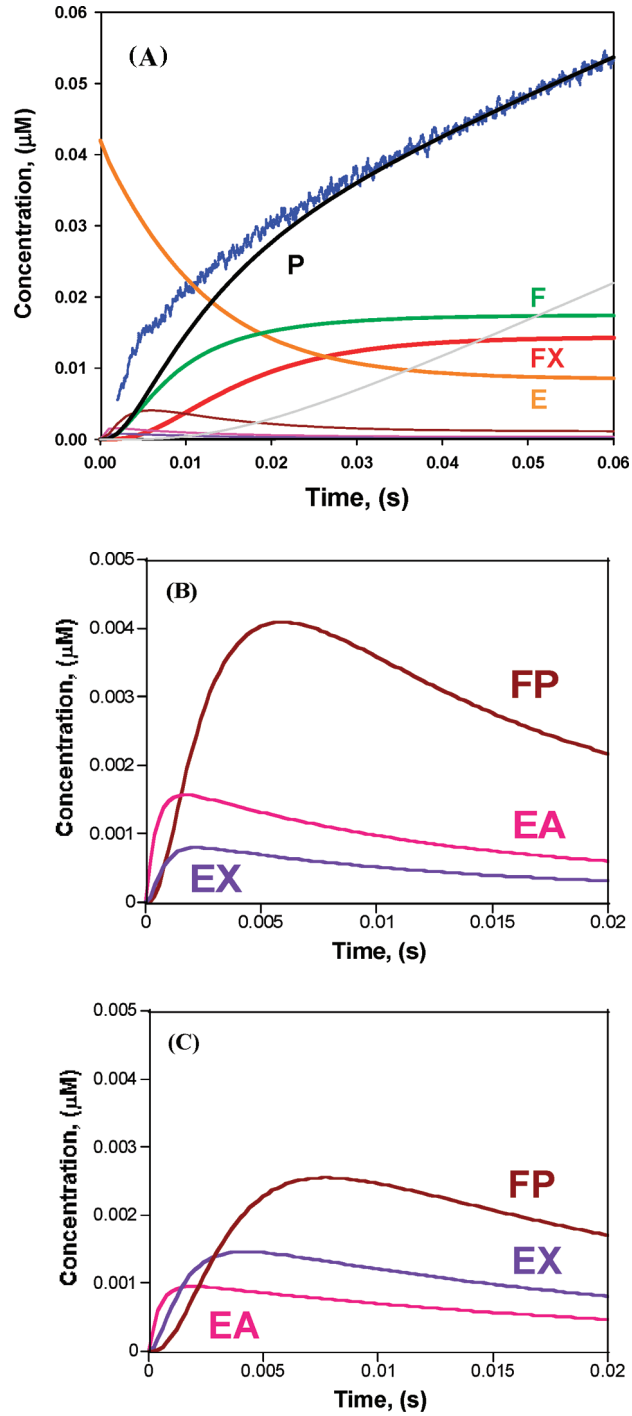

FIGURE 6: Simulations of time courses for the formation and disintegration of all enzyme, substrate, and product species formed during catalysis using 5 μM substrate and 42 nM cathepsin C. Scheme 1 was used as the model chemical mechanism, and values for all 13 rate constants, listed in Table 3, were used to simulate the reaction from 0 to 60 ms: free AMC product, P (black); free enzyme, E (orange); enzyme−substrate complex, EA (pink); enzyme intermediate, EX (purple); acylated enzyme−product complex, FP (brown); acylated enzyme, F (green); acylated enzyme intermediate, FX (red); and dipeptide product, Q (gray). There is no significant production or presence of enzyme dipeptide product, EQ, so it is not shown. (A) Plot of all enzyme species. Experimental data for 5 μM SY-AMC are shown in blue. During the steady state (>30 ms), the concentrations of F, FX, and E are 18 nM (43% of E_t), 14 nM (33% of E_t), and 8.6 nM (20% of E_t), respectively. (B) Levels of EA, EX, and FP formed in H_2O during the first 20 ms. (C) Levels of EA, EX, and FP formed in D_2O during the first 20 ms.

rate constants indicate that the formation of the tetrahedral complex in FX ($k_9 = 115\ s^{-1}$) is more rapid than its conversion to E′Q ($k_{11} = 36\ s^{-1}$), for which significant, normal intrinsic kinetic isotope effects ($^{D}k_9 = 2.6$ and $^{D}k_{11} = 3.2$) are determined. These would be expected on the slower steps in the deacylation half-reaction because of the general base hydrolysis of the acyl-bound enzyme which involves one primary and two secondary isotope effects on each of the two steps. This is also evident in Figure 6 as FX constitutes a long-lived complex in the generated time courses.

In summary, this work shows that integration of steady-state with both pre-steady-state kinetics and solvent kinetic isotope effects allowed the derivation of an almost complete kinetic picture of catalysis by a cysteine protease. This work also allows resolution of the relative levels of enzyme forms present during catalysis and, thus, combined with the chemical mechanisms involved, a potential roadmap to help steer drug discovery efforts for this and other disease-relevant cysteine proteases.

ACKNOWLEDGMENT

We thank Dr. Joseph Boyer for assistance in data fitting, Grace Chalypowicz, John Trill, and Maggie Grimes for the cloning and expression of the cathepsin C protein, and Dr. Jacques Briand for analysis of D_2O content of samples.

REFERENCES

1. Vasiljeva, O., Reinheckel, T., Peters, C., Turk, D., Turk, V., and Turk, B. (2007) Emerging roles of cysteine cathepsins in disease and their potential as drug targets. *Curr. Pharm. Des. 13*, 387–403.
2. Gelb, B. D., Shi, G. P., Chapman, H. A., and Desnick, R. J. (1996) Pycnodysostosis, a lysosomal disease caused by cathepsin K deficiency. *Science 273*, 1236–1238.
3. Stoch, S. A., and Wagner, J. A. (2008) Cathepsin K Inhibitors: A Novel Target for Osteoporosis Therapy. *Clin. Pharmacol. Ther. 83*, 172–176.
4. Yamashita, D. S., Marquis, R. W., Xie, R., Nidamarthy, S. D., Oh, H. J., Jeong, J. U., Erhard, K. F., Ward, K. W., Roethke, T. J., Smith, B. R., Cheng, H. Y., Geng, X., Lin, F., Offen, P. H., Wang, B., Nevins, N., Head, M. S., Haltiwanger, R. C., Narducci Sarjeant, A. A., Liable-Sands, L. M., Zhao, B., Smith, W. W., Janson, C. A., Gao, E., Tomaszek, T., McQueney, M., James, I. E., Gress, C. J., Zembryki, D. L., Lark, M. W., and Veber, D. F. (2006) Structure activity relationships of 5-, 6-, and 7-methyl-substituted azepan-3-one cathepsin K inhibitors. *J. Med. Chem. 49*, 1597–1612.
5. Adkison, A. M., Raptis, S. Z., Kelley, D. G., and Pham, C. T. (2002) Dipeptidyl peptidase I activates neutrophil-derived serine proteases and regulates the development of acute experimental arthritis. *J. Clin. Invest. 109*, 363–371.
6. Mallen-St Clair, J., Pham, C. T., Villalta, S. A., Caughey, G. H., and Wolters, P. J. (2004) Mast cell dipeptidyl peptidase I mediates survival from sepsis. *J. Clin. Invest. 113*, 628–634.
7. Pagano, M. B., Bartioli, M. A., Ennis, T. L., Mao, D., Simons, P. M., Thompson, R. W., and Pham, C. T. (2007) Critical role of dipeptidyl peptidase I in neutrophil recruitment during the development of experimental abdominal aortic aneurysms. *Proc. Natl. Acad. Sci. U.S.A. 104*, 2855–2860.
8. Wolters, P. J., Pham, C. T., Muilenburg, D. J., Ley, T. J., and Caughey, G. H. (2001) Dipeptidyl Peptidase I Is Essential for Activation of Mast Cell Chymases, but Not Tryptases, in Mice. *J. Biol. Chem. 276*, 18551–18556.
9. Hart, T. C., Hart, P. S., Bowden, D. W., Michalec, M. D., Callison, S. A., Walker, S. J., Zhang, Y., and Firatli, E. (1999) Mutations of the cathepsin C gene are responsible for Papillon-Lefèvre syndrome. *J. Med. Genet. 36*, 881–887.
10. Hart, T. C., Hart, P. S., Michalec, M. D., Zhang, Y., Firatli, E., Van Dyke, T. E., Stabholz, A., Zlotogorski, A., Shapira, L., and Soskolne, W. A. (2000) Haim-Munk syndrome and Papillon-Lefèvre syndrome are allelic mutations in cathepsin C. *J. Med. Genet. 37*, 88–94.
11. Oballa, R. M., Truchon, J. F., Bayly, C. I., Chauret, N., Day, S., Crane, S., and Berthelette, C. (2006) A generally applicable method for assessing the electrophilicity and reactivity of diverse nitrile-containing compounds. *Bioorg. Med. Chem. Lett. 17*, 998–1002.
12. MacCoss, M., and Baillie, T. A. (2004) Organic Chemistry in Drug Discovery. *Science 303*, 1810–1813.
13. Polgar, L. (2004) Catalytic mechanisms of cysteine peptidases. In *Handbook of Proteolytic Enzymes* (Barrett, A. J. ,Rawlings, N. D., and Woessner, J. F., Eds.) 2nd ed., pp 1072−1079, Elsevier Academic Press, San Diego.
14. Polgar, L. (1979) Deuterium Isotope Effects on Papain Acylation: Evidence of Lack of General Base Catalysis and for Enzyme-Leaving Group Interactions. *Eur. J. Biochem. 98*, 369–374.
15. Creighton, D. J., Gessouroun, M. S., and Heapes, J. M. (1980) Is the Thiolate-Imidazolium Pair the Catalytically Important Form of Papain? *FEBS Lett. 110*, 319–322.
16. Wandinger, A., and Creighton, D. J. (1980) Solvent Isotope Effects on the Rates of Alkylation of Thiolamine Models of Papain. *FEBS Lett. 116*, 116–121.
17. Creighton, D. J., and Schamp, D. J. (1980) Solvent Isotope Effects on the Tautomerization Equilibria of Papain and Model Thiolamines. *FEBS Lett. 110*, 313–318.
18. Lewis, S. D., Johnson, F. A., and Shafer, J. A. (1976) Potentiometric Determination of Ionization at the Active Site of Papain. *Biochemistry 15*, 5009–5017.
19. Ascenzi, P., Aducci, P., Torroni, A., Amiconi, B., Menegatti, E., and Guaneri, M. (1987) The pH-dependence of pre-steady-state and steady-state kinetics for the papain-catalyzed hydrolysis of N-α-glycine p-nitrophenyl ester. *Biochim. Biophys. Acta 912*, 203–210.
20. Brocklehurst, K., Kowlessur, D., Patel, G., Templeton, W., Quigley, K., Thomas, E. W., Wharton, C. W., Willenbrock, F., and Szalweski, R. J. (1988) Consequences of Molecular Recognition in the S1-S2 Intersubsite Region of Papain for Catalytic-Site Chemistry. *Biochem. J. 250*, 761–722.
21. Roberts, R. (2005) Lysosomal Cysteine Protease: Structure, Function and Inhibition of Cathepsins. *Drug News Perspect. 18*, 605–614.
22. Turk, B., Turk, B., and Turk, D. (1997) Structural and functional aspects of papain-like cysteine proteinases and their protein inhibitors. *J. Biol. Chem. 378*, 141–151.
23. Pinitglang, S., Watts, A., Patel, M., Reid, J., Noble, M., Gul, S., Bokth, A., Naeem, A., Patel, H., Thomas, E., Sreedharan, S., Verma, C., and Brocklehurst, K. (1997) A Classical Enzyme Active Center Motif Lacks Catalytic Competence until Modulated Electrostatically. *Biochemistry 36*, 9968–9982.
24. Bone, R., and Wolfenden, R. (1985) Solvent Isotope Effects on Formation of Protease Complexes with Inhibitory Aldehydes, with an Appendix on the Determination of Fractionation Factors by NMR. *J. Am. Chem. Soc. 107*, 4772–4777.
25. Ascenzi, P., Bocedi, A., Visca, P., Antonini, G., and Gradoni, L. (2003) Catalytic properties of cysteine proteinases from *Trypanosoma cruzi* and *Leishmania infantum*: A pre-steady-state and steady-state study. *Biochem. Biophys. Res. Commun. 309*, 659–665.
26. Solowiej, J., Thomson, J. A., Ryan, K., Luo, C., He, M., Lou, J., and Murray, B. W. (2008) Steady-state and pre-steady-state kinetic evaluation of severe acute respiratory syndrome coronavirus (SARS-CoV) 3CLpro cysteine protease: Development of an ion-pair model for catalysis. *Biochemistry 47*, 2617–2630.
27. Lowe, G. (1976) The Cysteine Proteases. *Tetrahedron 32*, 291–302.
28. Palmer, J. T., Rasnick, D., Klaus, J. L., and Bromme, D. (1995) Vinyl Sulfones as Mechanism-Based Cysteine Protease Inhibitors. *J. Med. Chem. 38*, 3193–3196.
29. Stanley, P. (1989) Chinese hamster ovary cell mutants with multiple glycosylation defects for production of glycoproteins with minimal carbohydrate heterogeneity. *Mol. Cell. Biol. 9*, 377–383.
30. Fahrner, R. L., Whitney, D. H., Vanderlann, M., and Blank, G. S. (1999) Performance comparison of Protein A affinity-chromatography sorbents for purifying recombinant monoclonal antibodies. *Biotechnol. Appl. Biochem. 30*, 121–128.
31. Grant, S. K., Deckman, I. C., Minnich, M. D., Culp, J., Franklin, S., Dreyer, G. B., Tomaszek, T. A., Jr., Debouck, C., and Meek, T. D. (1991) Purification and Biochemical Characterization of Recombinant Simian Immunodeficiency Virus Protease and Comparison to Human Immunodeficiency Virus Type 1 Protease. *Biochemistry 30*, 8424–8434.

32. Ellis, K. J., and Morrison, J. F. (1982) Buffers of constant ionic strength for studying pH-dependent processes. *Methods Enzymol. 87*, 405–426.
33. Schowen, K. B., and Schowen, R. L. (1982) Solvent Isotope Effects on Enzyme Systems. *Methods Enzymol. 87*, 551–606.
34. Johnson, K. A. (1983) The Pathway of ATP Hydrolysis by Dynein. *J. Biol. Chem. 258*, 13825–13832.
35. Cleland, W. W. (1975) Partition Analysis and Concept of Net Rate Constants As Tools In Enzyme Kinetics. *Biochemistry 14*, 3220–3224.
36. Quinn, D. M., and Sutton, L. D. (1991) Theoretical Basis and Mechanistic Utility of Solvent Isotope Effects. In *Enzyme Mechanisms from Isotope Effects* (Cook, P. F., Ed.) pp 73−127, CRC Press, Boca Raton, FL.
37. Knuckley, B., Bhatia, B., and Thompson, P. R. (2007) Protein Arginine Deiminase 4: Evidence for a Reverse Protonation Mechanism. *Biochemistry 46*, 6578–6587.
38. Moore, J. W., and Pearson, R. G. (1981) *Kinetics and Mechanism*, 3rd ed., pp 296−308, John Wiley & Sons, New York.
39. Palfey, B. A., and Fagan, R. L. (2006) Analysis of the Kinetic Isotope Effects on Initial Rates in Transient Kinetics. *Biochemistry 45*, 13631–13640.
40. Maniscalco, S. J., Tally, J. F., and Fisher, H. F. (2004) The Interpretation of Multiple-Step Transient-State Kinetic Isotope Effects. *Arch. Biochem. Biophys. 425*, 165–172.
41. Cook, P. F., and Cleland, W. W. (1981) Mechanistic Deductions from Isotope Effects in Multireactant Enzyme Mechanisms. *Biochemistry 20*, 1790–1796.
42. Northrop, D. B. (1977) Determining the Absolute Magnitude of Hydrogen Isotope Effects. In *Isotope Effects on Enzyme-Catalyzed Reactions* (Cleland, W. W., O'Leary, M. H., and Northrop, D. B., Eds.) pp 122−152, University Park Press, Baltimore.
43. Dolenc, I., Turk, B., Pungercic, G., Ritonja, A., and Turk, V. (1995) Oligomeric Structure and Substrate Induced Inhibition of Human Cathepsin C. *J. Biol. Chem. 270*, 21628–21631.
44. Molgaard, A., Arnau, J., Lauritzen, C., Larsen, S., Petersen, G., and Pedersen, J. (2007) The Crystal Structure of Human Dipeptidyl Peptidase (Cathepsin C) in Complex with the Inhibitor Gly-Phe-CHN2. *Biochem. J. 401*, 645–650.
45. Karsten, W. E., Lai, C. J., and Cook, P. F. (1995) Inverse Solvent Isotope Effects in the NAD-Malic Enzyme Reaction are the Result of the Viscosity Difference Between D_2O and H_2O: Implications for Solvent Isotope Effects Studies. *J. Am. Chem. Soc. 117*, 5914–5918.
46. Cook, P. F., Blanchard, J. S., and Cleland, W. W. (1980) Primary and secondary deuterium isotope effects on equilibrium constants for enzyme-catalyzed reactions. *Biochemistry 19*, 4853–4858.
47. Dahl, S. W., Halkier, T., Lauritzen, C., Dolenc, I., Pedersen, J., Turk, V., and Turk, B. (2001) Human Recombinant Pro-dipeptidyl Peptidase I (Cathepsin C) Can Be Activated by Cathepsins L and S but Not by Autocatalytic Processing. *Biochemistry 40*, 1671–1678.
48. Cleland, W. W., Hess, A., Robert, A., and Hengge, A. C. (1998) Isotope Effects on Enzyme-Catalyzed Acyl Transfer from p-Nitrophenyl Acetate: Concerted Mechanisms and Increased Hyperconjugation in the Transition State. *J. Am. Chem. Soc. 120*, 2703–2709.

BI8007627